ELSEVIER

International Journal of Solids and Structures 41 (2004) 199–226

INTERNATIONAL JOURNAL OF SOLIDS and STRUCTURES

www.elsevier.com/locate/ijsolstr

Continuous hyperplastic critical state (CHCS) model Derivation

I. Einav [a,*], A.M. Puzrin [b]

[a] *Centre for Offshore Foundation Systems, University of Western Australia, UWA Crawley, 6009 Perth, WA, Australia* [1]

[b] *School of Civil and Environmental Engineering, Georgia Institute of Technology, 790 Atlantic Drive, Atlanta, GA 30332-0355, USA* [1]

Received 14 January 2003; received in revised form 16 June 2003; accepted 3 September 2003

Abstract

The *hyperplasticity* and *continuous hyperplasticity* formulations enable complete derivation of thermodynamically admissible constitutive models. In this paper these two formulations are unified. This facilitates derivation of new forms of thermodynamical models that exhibit both global continuous behavior and the phenomenon of abrupt stiffness change within a single package. The concept allows for development of a technique for modeling of different kinematic stiffness regions bounded within an outer isotropic hardening yield surface, as observed in clays. This feature is employed for derivation of a new continuous hyperplastic critical state model. In general, this paper demonstrates how the specification of two potential functionals allows derivation of constitutive models that satisfy the Laws of Thermodynamics and at the same time account for many important aspects of soil behavior.

Keywords: Hyperplasticity; Continuous hyperplasticity; Generalized thermodynamics; Clays; Kinematic stiffness regions; Pressure dependent elasticity

1. Introduction

Many plasticity theories have been proposed over the years. While some theories are 'flexible enough' to cause violation of either the First and/or Second Law of Thermodynamics, some rigorous thermodynamic frameworks have also been developed over the years. The latter includes the rationalized thermodynamics (Coleman's classical paper, 1964; Truesdell's standard exposition, 1969) and the generalized thermodynamics—or thermodynamics of internal variables (Lubliner, 1972; Halphen and Nguyen Quoc Son, 1975, Ziegler, 1977, 1983; Maugin, 1992). Though the rationalized thermodynamics achieves considerable generality through the use of *functionals*, it has the disadvantage of being difficult to use in simple models that show abrupt events, such as yielding that occurs in conventional plasticity models. In contrast, whilst generalized thermodynamics has been a very successful in simulating such simple models, many materials

* Corresponding author. Tel.: +61-8-9380-7233; fax: +61-8-9380-1044.
E-mail address: einav@cyllene.uwa.edu.au (I. Einav).
[1] Formerly Israel Institute of Technology.

0020-7683/$ - see front matter © 2003 Elsevier Ltd. All rights reserved.
doi:10.1016/j.ijsolstr.2003.09.012

are known to exhibit a smoother behavior, that could not be simulated by discrete representation (Coleman and Gurtin, 1967; Kestin and Rice, 1970; Lubliner, 1972). According to Coleman and Gurtin, theories that rest on a finite number of internal state variables always linearize the spectra of behavior. Generalized thermodynamics, in that sense, over-simplifies the response by condensing the past history into the present of a finite number of internal variables; they being the amounts of energy associated with the various modes of molecular motion.

Puzrin and Houlsby (2001a,b) suggested an alternative to bypass these drawbacks of either generalized thermodynamics or rationalized thermodynamics, in the form of *continuous hyperplasticity*. The roots of this work can be related to the work of Ziegler (1977, 1983), Houlsby (1981), Collins and Houlsby (1997) and Houlsby and Puzrin (2000) who have also termed generalized thermodynamics models within this category as being *hyperplastic*; in analogues to *hyperelasticity*, such models are completely defined by thermodynamic potential functions. The basis for the *continuous hyperplastic* approach is still the generalized thermodynamics. However, in *continuous hyperplasticity* we make use of functionals, instead of functions, while the formulation preserves the concept of internal functions (instead of variables). While in the rationalized thermodynamics the *functionals* appear as functions of the past strain or temperature history, in *continuous hyperplasticity* the potentials are functions of the internal function.

As described by Puzrin and Houlsby, *continuous hyperplasticity* enables simulation of the smooth non-linear behavior exhibited by many materials, which could not be simulated by the discrete representation of *hyperplasticity*. There are some abrupt phenomena, however, that are better approached by discrete yielding rather than continuous yielding. For example, the isotropic hardening behavior of soils is seen as dependent upon a single yielding event (see Fig. 1 for both sand and clay); yet, before this yielding occurs the material introduces non-linearity, which is even implied by the "curvature (?)" question in Fig. 1a and which is very pronounced in the unloading curve in Fig. 1b.

The objective of this paper is to formulate a new thermodynamically admissible constitutive model which will hopefully compete with other existing non-thermomechanical constitutive models that are found in the literature. [2] In the course of providing such a model we develop some new concepts and constitutive modeling guidelines. Unifying the formulations of *hyperplasticity* and *continuous hyperplasticity* may suggest a single package, where both continuous behavior prior to the single instantaneous yielding and the monotonic behavior beyond this yielding are taken into account. The formulation we present in Section 2 is constructed particularly to capture this soil aspect, but could most probably be modified to enable other types of abrupt effects in different continuous materials.

The unified thermomechanical formulation requires a careful treatment of the incremental response and its drift corrected form as we do in Section 3. As mentioned earlier, prior to the instantaneous yielding of the soil, its behavior is non-linear. As suggested by Jardine (1992) among others, in clays this non-linearity should be described by a scheme of surfaces, bounding different kinematic regions. In Section 4 we develop a technique for modeling the kinematic stiffness-regions within the unified thermomechanical framework. A new continuous hyperplastic critical state (CHCS) model, which utilizes the above developments, is then derived from definition of only two potential functionals in Sections 5–7. Although the model is based on the unified thermomechanical formulation that allows modelling both continuous and abrupt phenomena, we term it "continuous" to emphasize its ability to "remember" continuously the history of loading events. As mentioned above, the model can also cope with the various distinct regimes in the history of the soil deformation, but the memory of the loading within the different regimes is always continuous.

Another important feature of the new model is that it adopts a new class of energy potential functions that allow for the well-known power dependency of elastic moduli on pressure to be generated without violation of the law of energy conservation. In addition, as described in Section 7, the model introduces a

[2] This statement is examined in a second part paper that is published separately (Einav and Puzrin, 2003b).

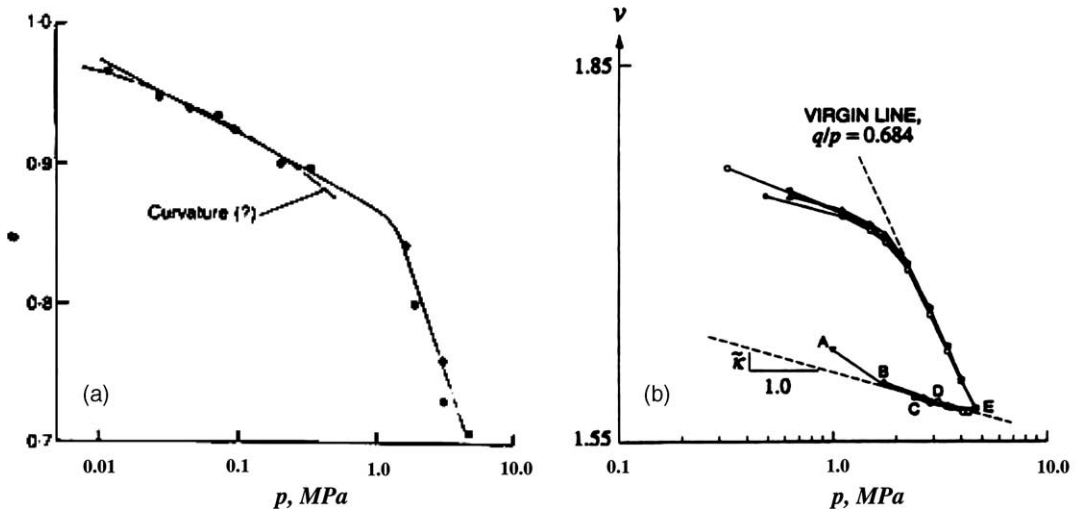

Fig. 1. Critical-state of: (a) Leighton Buzzard sand (Been et al., 1991) and (b) Vallerica clay (Borja et al., 1997).

special form of yield functions that account for the effects of the third stress invariant. In general, this paper will demonstrate how the specification of two potential functionals allows derivation of constitutive models that satisfy the Laws of Thermodynamics and at the same time account for many important aspects of soil behavior.

This paper also presents, in Section 8, a short parametric study that demonstrates to which parameters the model response is more sensitive. For more elaborate evaluation, on both laboratory and full geotechnical problem scales, readers are referred to the companion paper, which will be published separately.

2. A unified thermodynamical framework

The First Law of Thermodynamics states that there is an internal energy per unit volume u, which may be expressed in local rate form as

$$\boldsymbol{\sigma} : \dot{\boldsymbol{\varepsilon}} - \nabla \cdot \boldsymbol{h} = \dot{u} \tag{1}$$

where $\boldsymbol{\sigma}$ is the effective Cauchy stress tensor; $\dot{\boldsymbol{\varepsilon}}$ is the small strain tensor; $\boldsymbol{h}$ is the heat flow-vector; the first term is the mechanical work input; the second term is the rate of heat supply to the material element from its surroundings; we use the Nabla operator to indicate the spatial differential and the symbol ":" denotes the inner product of two second-order tensors.

The Second Law of Thermodynamics can be expressed by the entropy scalar property S such that $\dot{S} \geqslant -\nabla \cdot (\boldsymbol{h}/\theta)$, where θ is the local absolute temperature and $-\nabla \cdot (\boldsymbol{h}/\theta)$ is the entropy flux, i.e., the reversible part of entropy change. The Law can be restated as

$$\underbrace{\theta \dot{S} + \nabla \cdot \boldsymbol{h}}_{d} - \frac{\boldsymbol{h} \cdot \nabla \theta}{\theta} \geqslant 0$$

The first two terms represent the mechanical dissipation d, the third term $-\frac{\boldsymbol{h} \cdot \nabla \theta}{\theta}$ is called the thermal dissipation and is always non-negative by virtue of the fact that the heat flux is always in the direction of the

negative thermal gradient. The thermal dissipation decreases by comparison with the mechanical dissipation for slow processes, so it is argued that the mechanical dissipation must itself be non-negative

$$\theta\dot{S} + \nabla \cdot \boldsymbol{h} \equiv d \geqslant 0 \tag{2}$$

This is a slightly more stringent condition, but it is widely accepted and referred to as Plank's inequality (see Truesdell, 1969). From (1) and (2) it follows that:

$$\dot{u} = \boldsymbol{\sigma} : \dot{\boldsymbol{\varepsilon}} + \theta\dot{S} - d \tag{3}$$

In the formulation of *hyperplasticity* (Collins and Houlsby, 1997; Houlsby and Puzrin, 2000) the internal energy, being a function of state, is assumed to depend on strain, an internal variable $\boldsymbol{\alpha}$ and entropy, thus $u = u(\boldsymbol{\varepsilon}, S, \boldsymbol{\alpha})$. In the formulation of *continuous hyperplasticity* (Puzrin and Houlsby, 2001a,b) the internal variable is replaced by an internal function $\hat{\boldsymbol{\alpha}} \equiv \hat{\boldsymbol{\alpha}}(\eta)$, $\eta \in D$, where η is its internal coordinate in the domain D, such that $u = u[\boldsymbol{\varepsilon}, S, \hat{\boldsymbol{\alpha}}]$, while the square brackets [] denote that internal energy is now a functional of state, rather than a function of state.

For the purpose of this work, let us assume that the internal energy is a functional of both the internal variable and the internal function, such that

$$\dot{u} = \dot{u}[\boldsymbol{\varepsilon}, S, \boldsymbol{\alpha}^*, \hat{\boldsymbol{\alpha}}] = \frac{\partial u}{\partial \boldsymbol{\varepsilon}} : \dot{\boldsymbol{\varepsilon}} + \frac{\partial u}{\partial S}\dot{S} - \bar{\boldsymbol{\chi}}^* \bullet \dot{\boldsymbol{\alpha}}^* - \int_D (\hat{\bar{\boldsymbol{\chi}}} \bullet \dot{\hat{\boldsymbol{\alpha}}})\,\mathrm{d}\eta \tag{4}$$

where we denote $\bar{\boldsymbol{\chi}}^* = -\frac{\partial u}{\partial \boldsymbol{\alpha}^*}$ and $\hat{\bar{\boldsymbol{\chi}}} = -\frac{\partial u}{\partial \hat{\boldsymbol{\alpha}}}$ as the *hyperplastic* and *continuous hyperplastic* generalized stresses; the upper case asterisk sign was added to the internal variable associated with the *hyperplastic* component, in order to differentiate it more clearly from the internal function $\hat{\boldsymbol{\alpha}}(\eta)$. Since internal variable (or function) can be a scalar, tensor, or a collection of scalars and tensors of various orders, we introduce the use of the bold dot "$\bullet$" to designate a general inner product of two general variables. Once the structure of $\boldsymbol{\alpha}^*$ and $\hat{\boldsymbol{\alpha}}$ is known, the operator "$\bullet$" may be interpreted accordingly. For example, if $\boldsymbol{\alpha}^*$ is a vector-like variable, $\frac{\partial u}{\partial \boldsymbol{\alpha}^*} \bullet \dot{\boldsymbol{\alpha}}^*$ corresponds to the vector product $\frac{\partial u}{\partial \boldsymbol{\alpha}^*} \cdot \dot{\boldsymbol{\alpha}}^*$, if it is a tensor-like variable the operator corresponds to $\frac{\partial u}{\partial \boldsymbol{\alpha}^*} : \dot{\boldsymbol{\alpha}}^*$.

Assuming that the dissipation is a function of the thermodynamic state of the material as well as of the rate of change of internal variable (or function), and considering only isothermal mechanisms where isotropic hardening is due only to the single *hyperplastic* component, we restrict

$$d^e = d^{e^*}(\boldsymbol{\psi}, \boldsymbol{\alpha}^*, \dot{\boldsymbol{\alpha}}^*) + \int_D \hat{d}^e[\boldsymbol{\psi}, \boldsymbol{\alpha}^*, \dot{\hat{\boldsymbol{\alpha}}}(\eta), \eta] \geqslant 0 \tag{5}$$

where we introduce

$$\boldsymbol{\psi} = \begin{cases} \boldsymbol{\varepsilon} \text{ for } (u) \text{ and } (f) \text{ formulations} \\ \boldsymbol{\sigma} \text{ for } (h) \text{ and } (g) \text{ formulations} \end{cases}$$

In each combination the superscript e over d denotes a type of energy potential with which d is associated, while u, f, h, and g correspond to internal energy, Helmholtz free energy, enthalpy and Gibbs free energy potentials. Although, at this stage we have only defined the internal energy u, the use of the alternative forms will be clarified below. Note also that d^{e^*} and $\hat{d}^e$ corresponds to the *hyperplastic* and *continuous hyperplastic* components.

Euler's theorem for rate independent materials gives

$$d^e = \frac{\partial d^e}{\partial \dot{\boldsymbol{\alpha}}^*} \bullet \dot{\boldsymbol{\alpha}}^* + \int_D \frac{\partial \hat{d}^e}{\partial \dot{\hat{\boldsymbol{\alpha}}}} \bullet \dot{\hat{\boldsymbol{\alpha}}}\,\mathrm{d}\eta = \boldsymbol{\chi}^* \bullet \dot{\boldsymbol{\alpha}}^* + \int_D \hat{\boldsymbol{\chi}} \bullet \dot{\hat{\boldsymbol{\alpha}}}\,\mathrm{d}\eta \geqslant 0 \tag{6}$$

where $\boldsymbol{\chi}^* = \frac{\partial d^e}{\partial \dot{\boldsymbol{\alpha}}^*}$ and $\hat{\boldsymbol{\chi}} = \frac{\partial \hat{d}^e}{\partial \dot{\hat{\boldsymbol{\alpha}}}}$ denote the dissipative generalized stresses of the *hyperplastic* and *continuous hyperplastic* components in that order. Adding Eqs. (3), (4) and (6) it could be easily verified that

$$\left(\boldsymbol{\sigma}-\frac{\partial u}{\partial \boldsymbol{\varepsilon}}\right):\dot{\boldsymbol{\varepsilon}}+\left(\theta-\frac{\partial u}{\partial S}\right)\dot{S}+(\bar{\boldsymbol{\chi}}^{*}-\boldsymbol{\chi}^{*})\bullet\dot{\boldsymbol{\alpha}}^{*}+\int_{D}(\hat{\bar{\boldsymbol{\chi}}}-\hat{\boldsymbol{\chi}})\bullet\dot{\hat{\boldsymbol{\alpha}}}\,\mathrm{d}\eta=0$$

where by assuming Ziegler's normality condition in the form $\bar{\boldsymbol{\chi}}^{*}=\boldsymbol{\chi}^{*}$ and $\hat{\bar{\boldsymbol{\chi}}}(\eta)=\hat{\boldsymbol{\chi}}(\eta)$, $\forall\eta\in D$, the Coleman relations

$$\boldsymbol{\sigma}=\frac{\partial u}{\partial \boldsymbol{\varepsilon}};\quad \theta=\frac{\partial u}{\partial S} \tag{7}$$

are validated since $\dot{\boldsymbol{\varepsilon}}$ and $\dot{S}$ are state variables rates, that can be specified arbitrarily in a given thermodynamic state (Einav (2002) for discussion).

2.1. Energy potentials

The first equation in (7) suggests the existence of the enthalpy energy potential through Legendre transformation in the form: $h[\boldsymbol{\sigma},\boldsymbol{\alpha}^{*},\hat{\boldsymbol{\alpha}},S]=u[\boldsymbol{\varepsilon},\boldsymbol{\alpha}^{*},\hat{\boldsymbol{\alpha}},S]-\boldsymbol{\sigma}:\boldsymbol{\varepsilon}$; the second equation in (7) suggests the existence of the Helmholtz free energy potential through Legendre transformation in the form: $f[\boldsymbol{\varepsilon},\boldsymbol{\alpha}^{*},\hat{\boldsymbol{\alpha}},\theta]=u[\boldsymbol{\varepsilon},\boldsymbol{\alpha}^{*},\hat{\boldsymbol{\alpha}},S]-S\theta$; this relation implies $\boldsymbol{\sigma}=\partial u/\partial\boldsymbol{\varepsilon}=\partial f/\partial\boldsymbol{\varepsilon}$, which in return suggests another energy potential, this time the Gibbs free energy through Legendre transformation in the form: $g[\boldsymbol{\sigma},\boldsymbol{\alpha}^{*},\hat{\boldsymbol{\alpha}},\theta]=f[\boldsymbol{\varepsilon},\boldsymbol{\alpha}^{*},\hat{\boldsymbol{\alpha}},\theta]-\boldsymbol{\sigma}:\boldsymbol{\varepsilon}$; this relation implies $\boldsymbol{\varepsilon}=-\partial g/\partial\boldsymbol{\sigma}$. In all of these transformations the internal variable/function was passive, thus the generalized stresses may be defined alternatively by

$$\left.\begin{aligned}\hat{\bar{\boldsymbol{\chi}}}&=-\frac{\partial u}{\partial\hat{\boldsymbol{\alpha}}}=-\frac{\partial h}{\partial\hat{\boldsymbol{\alpha}}}=-\frac{\partial f}{\partial\hat{\boldsymbol{\alpha}}}=-\frac{\partial g}{\partial\hat{\boldsymbol{\alpha}}}\qquad\forall\eta\in D\\ \bar{\boldsymbol{\chi}}^{*}&=-\frac{\partial u}{\partial\boldsymbol{\alpha}^{*}}=-\frac{\partial h}{\partial\boldsymbol{\alpha}^{*}}=-\frac{\partial f}{\partial\boldsymbol{\alpha}^{*}}=-\frac{\partial g}{\partial\boldsymbol{\alpha}^{*}}\end{aligned}\right\} \tag{8}$$

In the particular case where the Gibbs free energy potential takes the isothermal form of

$$g[\boldsymbol{\sigma},\boldsymbol{\alpha}^{*},\hat{\boldsymbol{\alpha}}]=g_{1}(\boldsymbol{\sigma})-\boldsymbol{\sigma}:\left(\int_{D}\hat{\boldsymbol{\alpha}}\,\mathrm{d}\eta+\boldsymbol{\alpha}^{*}\right)+\int_{D}\hat{g}_{2}(\hat{\boldsymbol{\alpha}},\eta)\,\mathrm{d}\eta \tag{9}$$

we restrict our study to the temperature independent processes where the strain can be decomposed into elastic and plastic components by

$$\boldsymbol{\varepsilon}=-\frac{\partial g}{\partial\boldsymbol{\sigma}}=\underbrace{-\frac{\partial g_{1}(\boldsymbol{\sigma})}{\partial\boldsymbol{\sigma}}}_{\boldsymbol{\varepsilon}_{\mathrm{e}}}+\underbrace{\boldsymbol{\alpha}^{*}+\int_{D}\hat{\boldsymbol{\alpha}}\,\mathrm{d}\eta}_{\boldsymbol{\varepsilon}_{\mathrm{p}}} \tag{10}$$

where coupling between internal variables may occur.

Noting Eq. (8), for this special case, the generalized stress function becomes:

$$\hat{\bar{\boldsymbol{\chi}}}=\boldsymbol{\sigma}-\hat{\boldsymbol{\rho}}(\hat{\boldsymbol{\alpha}});\quad\hat{\bar{\boldsymbol{\chi}}}^{*}=\boldsymbol{\sigma} \tag{11}$$

where $\hat{\boldsymbol{\rho}}\equiv\partial\hat{g}_{2}/\partial\hat{\boldsymbol{\alpha}}$ is the "back stress" associated with the internal function, and we permit no kinematic translation of the hyperplastic component of the model since $\boldsymbol{\rho}^{*}\equiv\partial g_{2}^{*}/\partial\boldsymbol{\alpha}^{*}=0$.

2.2. Yield surfaces and dissipation

The dissipation in Eq. (6) suggests that the first component is related to a single hyperplastic surface through the degenerate special case of the Legendre transformation

$$\lambda^{*}y^{e^{*}}=\boldsymbol{\chi}^{*}\bullet\dot{\boldsymbol{\alpha}}^{*}-d^{e^{*}}=0 \tag{12}$$

where λ^{*} is the consistency parameter satisfying the Kuhn–Tucker complementary conditions in the form $\{\lambda^{*}\geqslant 0,y^{e^{*}}\leqslant 0,\lambda^{*}y^{e^{*}}=0\}$, and $y^{e^{*}}$ is the yield function in the form

$$y^{e^*} = y^{e^*}(\boldsymbol{\psi}, \boldsymbol{\alpha}^*, \boldsymbol{\chi}^*) \leqslant 0 \tag{13}$$

The functional component in Eq. (6) is converted into a field of yield surfaces, through the relation

$$\hat{\lambda}\hat{y}^e = \hat{\boldsymbol{\chi}} \bullet \dot{\hat{\boldsymbol{\alpha}}} - \hat{d}^e = 0 \quad \forall \eta \in D \tag{14}$$

where $\hat{\lambda} \equiv \hat{\lambda}(\eta)$ satisfies the Kuhn–Tucker conditions in the form $\{\hat{\lambda} \geqslant 0, \hat{y}^e \leqslant 0, \hat{\lambda}\hat{y}^e = 0\}$, and $\hat{y}^e$ is the corresponding continuous field of yield functions in the form:

$$\hat{y}^e = \hat{y}^e(\boldsymbol{\psi}, \boldsymbol{\alpha}^*, \hat{\boldsymbol{\chi}}, \eta) \leqslant 0 \quad \forall \eta \in D \tag{15}$$

where $\hat{y}^e(\boldsymbol{\psi}, \boldsymbol{\alpha}^*, \hat{\boldsymbol{\chi}}, \eta) = 0$ is the η-coordinate yield surface.

The dependence of both y^{e^*} and $\hat{y}^e$ on the same internal variable $\boldsymbol{\alpha}^*$, suggests that all surfaces may experience isotropic hardening, which depends upon a single instantaneous yielding event of the hyperplastic yield function in (13); hence, we name the surface $y^{e^*} = 0$ as the isotropic hardening yield surface.

3. Incremental response

For simplicity, let us derive the incremental response for g-formulation only. From the time differentiation of the generalized stresses (11) it follows that

$$\dot{\hat{\boldsymbol{\chi}}} = \dot{\boldsymbol{\sigma}} - \frac{\partial^2 \hat{g}_2}{\partial \hat{\boldsymbol{\alpha}} \partial \hat{\boldsymbol{\alpha}}} : \dot{\hat{\boldsymbol{\alpha}}} \quad \forall \eta \in D \tag{16}$$

$$\dot{\boldsymbol{\chi}}^* = \dot{\boldsymbol{\sigma}} \tag{17}$$

The consistency condition for the isotropic hardening/softening yield surface is obtained by time differentiation of (13) for the limiting equality case

$$\dot{y}^{g^*} = \dot{y}^{g^*}(\boldsymbol{\sigma}, \boldsymbol{\alpha}^*, \boldsymbol{\chi}^*) = \frac{\partial y^{g^*}}{\partial \boldsymbol{\sigma}} : \dot{\boldsymbol{\sigma}} + \frac{\partial y^{g^*}}{\partial \boldsymbol{\alpha}^*} : \dot{\boldsymbol{\alpha}}^* + \frac{\partial y^{g^*}}{\partial \boldsymbol{\chi}^*} : \dot{\boldsymbol{\chi}}^* = 0 \tag{18}$$

and that of the field of yield surfaces is given by differentiating equation (15) for the limiting equality case

$$\dot{\hat{y}}^g = \dot{\hat{y}}^g(\boldsymbol{\sigma}, \boldsymbol{\alpha}^*, \hat{\boldsymbol{\chi}}, \eta) = \frac{\partial \hat{y}^g}{\partial \boldsymbol{\sigma}} : \dot{\boldsymbol{\sigma}} + \frac{\partial \hat{y}^g}{\partial \boldsymbol{\alpha}^*} : \dot{\boldsymbol{\alpha}}^* + \frac{\partial \hat{y}^g}{\partial \hat{\boldsymbol{\chi}}} : \dot{\hat{\boldsymbol{\chi}}} = 0, \quad \forall \eta \in D \tag{19}$$

From the properties of the Legendre transformation in (12) it follows that the flow rule for the isotropic surface is

$$\dot{\boldsymbol{\alpha}}^* = \lambda^* \frac{\partial y^{e^*}}{\partial \boldsymbol{\chi}^*} \tag{20}$$

where the flow rule for the field of yield surfaces is given from the properties of (14) by

$$\dot{\hat{\boldsymbol{\alpha}}} = \hat{\lambda} \frac{\partial \hat{y}^e}{\partial \hat{\boldsymbol{\chi}}} \quad \forall \eta \in D \tag{21}$$

The combination of Eqs. (17), (18) and (20) provides a solution for the non-negative plasticity multiplier of the *hyperplastic* isotropic hardening/softening yield surface

$$\lambda^* = \frac{-\left(\dfrac{\partial y^{g^*}}{\partial \boldsymbol{\chi}^*} + \dfrac{\partial y^{g^*}}{\partial \boldsymbol{\sigma}}\right) : \dot{\boldsymbol{\sigma}}}{\dfrac{\partial y^{g^*}}{\partial \boldsymbol{\chi}^*} : \dfrac{\partial y^{g^*}}{\partial \boldsymbol{\alpha}^*}} \tag{22}$$

The solution for the non-negative plasticity multiplier function of the field of *continuous hyperplastic* yield surfaces is a function of the solution of λ^* in (22), and is given by

$$\hat{\lambda} = \frac{\left(\frac{\partial \hat{y}^g}{\partial \hat{\boldsymbol{\chi}}} + \frac{\partial \hat{y}^g}{\partial \boldsymbol{\sigma}}\right) : \dot{\boldsymbol{\sigma}} + \lambda^* \frac{\partial y^{g^*}}{\partial \boldsymbol{\chi}^*} : \frac{\partial \hat{y}^g}{\partial \boldsymbol{\alpha}^*}}{\frac{\partial \hat{y}^g}{\partial \hat{\boldsymbol{\chi}}} : \frac{\partial^2 \hat{g}_2}{\partial \hat{\boldsymbol{\alpha}} \partial \hat{\boldsymbol{\alpha}}} : \frac{\partial \hat{y}^g}{\partial \hat{\boldsymbol{\chi}}}} \quad \forall \eta \in D \tag{23}$$

which was obtained by rearrangement of Eqs. (16) and (19)–(21). This indicates the coupled dependency of the kinematic yield surfaces' plastic flow on the plastic flow of the isotropic hardening hyperplastic yield surface. Finally, the solution for the strain time rates is given by a derivation of (10)

$$\dot{\boldsymbol{\varepsilon}} = -\frac{\partial^2 g_1}{\partial \boldsymbol{\sigma} \partial \boldsymbol{\sigma}} : \dot{\boldsymbol{\sigma}} + \int_D \dot{\hat{\boldsymbol{\alpha}}} \mathrm{d}\eta + \dot{\boldsymbol{\alpha}}^* \tag{24}$$

If we substitute the generalized stresses (11) into the generalized yield surfaces (13) and (15) the yield surfaces in true stress space are extracted

$$\left.\begin{aligned} &y^{g^*}_{\mathrm{T}}(\boldsymbol{\sigma}, \boldsymbol{\alpha}^*) = y^{g^*}(\boldsymbol{\sigma}, \boldsymbol{\alpha}^*, \boldsymbol{\chi}^* \to \boldsymbol{\sigma}) \\ &\hat{y}^g_{\mathrm{T}}(\boldsymbol{\sigma}, \boldsymbol{\alpha}^*, \hat{\boldsymbol{\alpha}}, \eta) = \hat{y}^g(\boldsymbol{\sigma}, \boldsymbol{\alpha}^*, \hat{\boldsymbol{\chi}} \to \boldsymbol{\sigma} - \hat{\boldsymbol{\rho}}(\hat{\boldsymbol{\alpha}}), \eta) \quad \forall \eta \in D \end{aligned}\right\} \tag{25}$$

where the subscript 'T' is added to identify the true stress space yield surfaces from those of the generalized space.

Remark. If the $\eta = \breve{\eta}$ coordinate yield surface in D initially coincides with the isotropic hardening/softening surface in both true and generalized spaces, their first yielding occurs simultaneously, while $\hat{\boldsymbol{\alpha}}(\breve{\eta}) = \mathbf{0}$. Since at that moment $y^{g^*}(\boldsymbol{\sigma}, \boldsymbol{\alpha}^*, \boldsymbol{\chi}^*) = \hat{y}^g(\boldsymbol{\sigma}, \boldsymbol{\alpha}^*, \hat{\boldsymbol{\chi}}, \breve{\eta}) = 0$ as well, we observe the following equalities:

$$\left.\begin{aligned} &\partial \hat{y}^g / \partial \boldsymbol{\sigma}|_{\hat{\boldsymbol{\alpha}}(\breve{\eta})=\mathbf{0}} = \partial y^{g^*} / \partial \boldsymbol{\sigma} \\ &\partial \hat{y}^g / \partial \boldsymbol{\alpha}^*|_{\hat{\boldsymbol{\alpha}}(\breve{\eta})=\mathbf{0}} = \partial y^{g^*} / \partial \boldsymbol{\alpha}^* \\ &\partial \hat{y}^g / \partial \boldsymbol{\chi}^*|_{\hat{\boldsymbol{\alpha}}(\breve{\eta})=\mathbf{0}} = \partial y^{g^*} / \partial \boldsymbol{\chi}^* \end{aligned}\right\} \tag{26}$$

Implementing Eq. (26) with Eqs. (22) and (23) suggests that for this moment of yielding $\hat{\lambda}(\breve{\eta}) = 0$. Therefore, the first increment of the associated internal variable is $\dot{\hat{\boldsymbol{\alpha}}} = \hat{\lambda}(\breve{\eta}) \frac{\partial \hat{y}^g}{\partial \hat{\boldsymbol{\chi}}}(\breve{\eta}) = \mathbf{0}$. As a result, if the dependencies of both surfaces on $\boldsymbol{\alpha}^*$ are the same, Eq. (26) still hold and Eqs. (22) and (23) still give $\hat{\lambda}(\breve{\eta}) = 0$. The above reasoning continues inductively, so that we always get $\hat{\boldsymbol{\alpha}}(\breve{\eta}) \equiv \mathbf{0}$. The last observation will be of use while we formulate specific models within the formulation.

3.1. Drift corrected incremental response

The special incremental response we have presented also requires careful attention when converting it to the drift corrected version for a numerical algorithmised in a computer code. For this purpose we convert the above derivation into the discrete multi-surface hyperplasticity (Puzrin and Houlsby, 2001b) formulation as proposed by Einav et al. (2003). From a computational standpoint, continuous hyperplasticity is similar to the multi-surface hyperplasticity formulation. However, the characterization of the distribution function $H(\eta)$ is identified using the framework of continuous hyperplasticity and these formulations differ from each other conceptually. Note that the single hyperplastic component need not be dealt with in any exceptional manner. For that reason, the Gibbs free energy potential functional (Eq. (9)) is replaced by the function

$$g(\boldsymbol{\sigma},\boldsymbol{\alpha}^*,\boldsymbol{A}) = g_1(\boldsymbol{\sigma}) - \boldsymbol{\sigma} : \left(\sum_{n=1}^{N}\boldsymbol{\alpha}_n + \boldsymbol{\alpha}^*\right) + \sum_{n=1}^{N} g_{2,n}(\boldsymbol{\alpha}_n) \tag{27}$$

where $\boldsymbol{A} = \boldsymbol{A}(\boldsymbol{\alpha}_1,\ldots,\boldsymbol{\alpha}_N)$ is a set of internal variables, replacing the internal function $\hat{\boldsymbol{\alpha}} \equiv \hat{\boldsymbol{\alpha}}(\eta), \eta \in \{0,1\}$. While Eq. (17) still holds, Eq. (16) is replaced by

$$\dot{\overset{\sim}{\boldsymbol{\chi}}}_n = \dot{\boldsymbol{\sigma}} - \frac{\partial^2 g_{2,n}}{\partial\boldsymbol{\alpha}_n\partial\boldsymbol{\alpha}_n} : \dot{\boldsymbol{\alpha}}_n \quad \forall n \in \{1,\ldots,N\} \tag{28}$$

The consistency condition for the hyperplastic isotropic hardening surface is given by

$$\dot{y}^{g^*} = \dot{y}^{g^*}(\boldsymbol{\sigma},\boldsymbol{\alpha}^*,\boldsymbol{\chi}^*) = \frac{\partial y^{g^*}}{\partial\boldsymbol{\sigma}} : \dot{\boldsymbol{\sigma}} + \frac{\partial y^{g^*}}{\partial\boldsymbol{\alpha}^*} : \dot{\boldsymbol{\alpha}}^* + \frac{\partial y^{g^*}}{\partial\boldsymbol{\chi}^*} : \dot{\boldsymbol{\chi}}^* = -\delta^* \tag{29}$$

where $\delta^* = y^{g^*}(\boldsymbol{\sigma},\boldsymbol{\alpha}^*,\boldsymbol{\chi}^*)$ is added to (18) to correct the yield surface drift for a single hyperplastic surface.

The continuous field of yield surfaces in Eq. (15) could be represented by a discrete field of surfaces, given by

$$y_n^g = y_n^g(\boldsymbol{\sigma},\boldsymbol{\alpha}^*,\boldsymbol{\chi}_n,n/N) \quad \forall n \in \{1,2,\ldots,N\} \tag{30}$$

where a linear distribution n/N (see Einav et al., 2003) replaces η as the coordinate indicating the relative size of the yield surface compared to the largest yield surface at the nth position. The consistency condition of the nth surface is

$$\dot{y}_n^g = \dot{y}_n^g(\boldsymbol{\sigma},\boldsymbol{\alpha}^*,\boldsymbol{\chi}_n,n/N) = \frac{\partial y_n^g}{\partial\boldsymbol{\sigma}} : \dot{\boldsymbol{\sigma}} = \frac{\partial y_n^g}{\partial\boldsymbol{\alpha}^*} : \dot{\boldsymbol{\alpha}}^* + \frac{\partial y_n^g}{\partial\boldsymbol{\chi}_n} : \dot{\boldsymbol{\chi}}_n = -\delta_n \tag{31}$$

where $\delta_n = y_n^g(\boldsymbol{\sigma},\boldsymbol{\alpha}^*,\boldsymbol{\chi}_n,n/N)$ is supplemented to correct drifting of the nth yield surface.

Substitution of the flow rule for the isotropic hardening surface $\dot{\boldsymbol{\alpha}}^* = \lambda^* \frac{\partial y^{g^*}}{\partial\boldsymbol{\chi}^*}$ and of Eq. (17) into Eq. (29) leads to a solution of the drift corrected non-negative multiplier of the isotropic surface

$$\lambda^* = \frac{-\left(\dfrac{\partial y^{g^*}}{\partial\boldsymbol{\sigma}} + \dfrac{\partial y^{g^*}}{\partial\boldsymbol{\chi}^*}\right) : \dot{\boldsymbol{\sigma}} + \delta^*}{\dfrac{\partial y^{g^*}}{\partial\boldsymbol{\chi}^*} : \dfrac{\partial y^{g^*}}{\partial\boldsymbol{\alpha}^*}} \tag{32}$$

The solution for the nth non-negative multiplier of the nth kinematic yield surface is derived by combining the nth flow rule $\dot{\boldsymbol{\alpha}}_n = \lambda_n \frac{\partial y_n^g}{\partial\boldsymbol{\chi}_n}$, the isotropic-hardening-surface flow-rule $\dot{\boldsymbol{\alpha}}^* = \lambda^* \frac{\partial y^{g^*}}{\partial\boldsymbol{\chi}^*}$, the nth equation in (28), and the nth consistency condition (31):

$$\lambda_n = \frac{\left(\dfrac{\partial y_n^g}{\partial\boldsymbol{\chi}_n} + \dfrac{\partial y_n^g}{\partial\boldsymbol{\sigma}}\right) : \dot{\boldsymbol{\sigma}} + \lambda^* \dfrac{\partial y_n^g}{\partial\boldsymbol{\alpha}^*} : \dfrac{\partial y^{g^*}}{\partial\boldsymbol{\chi}^*} + \delta_n}{\dfrac{\partial y_n^g}{\partial\boldsymbol{\chi}_n} : \dfrac{\partial^2 g_{2,n}}{\partial\boldsymbol{\alpha}_n\partial\boldsymbol{\alpha}_n} : \dfrac{\partial y_n^g}{\partial\boldsymbol{\chi}_n}} \quad \forall n \in \{1,2\ldots,N\} \tag{33}$$

Finally, the multi-surface format of Eq. (24) is given by

$$\dot{\boldsymbol{\varepsilon}} = -\frac{\partial^2 g_1}{\partial\boldsymbol{\sigma}\partial\boldsymbol{\sigma}} : \dot{\boldsymbol{\sigma}} + \sum_{n=1}^{N}\dot{\boldsymbol{\alpha}}_n + \dot{\boldsymbol{\alpha}}^* \tag{34}$$

which together with the flow rules, Eqs. (32), (33), (17) and (28) constitute the drift corrected incremental response for stress controlled processes. Indeed, combining this with a general loading conditions equation in the form $\mathbf{C} : \dot{\boldsymbol{\sigma}} + \mathbf{D} : \dot{\boldsymbol{\varepsilon}} = \mathbf{S}$ suggests that

$$\left.\begin{aligned}\dot{\boldsymbol{\sigma}} &= \left[\mathbf{C}-\mathbf{D}:\left(\frac{\partial^2 g_1}{\partial\boldsymbol{\sigma}\partial\boldsymbol{\sigma}}-\sum_{i=1}^{N}\boldsymbol{L}_i\otimes\frac{\partial y_i^g}{\partial\boldsymbol{\chi}_i}-\boldsymbol{L}^*\otimes\frac{\partial y^{g^*}}{\partial\boldsymbol{\chi}^*}\right)\right]^{-1}:\left[\mathbf{S}+\sum_{i=1}^{N}\frac{\delta_i}{A_i}\frac{\partial y_i^g}{\partial\boldsymbol{\chi}_i}+\frac{\delta^*}{A^*}\frac{\partial y^{g^*}}{\partial\boldsymbol{\chi}^*}\right]\\ \dot{\boldsymbol{\varepsilon}} &= \mathbf{D}^{-1}:(\mathbf{S}-\mathbf{C}:\dot{\boldsymbol{\sigma}})\end{aligned}\right\} \tag{35}$$

where

$$A_n=\frac{\partial y_n^g}{\partial\boldsymbol{\chi}_n}:\frac{\partial^2 g_{2,n}}{\partial\boldsymbol{\alpha}_n\partial\boldsymbol{\alpha}_n}:\frac{\partial y_n^g}{\partial\boldsymbol{\chi}_n};\quad A^*=\frac{\partial y^{g^*}}{\partial\boldsymbol{\chi}^*}:\frac{\partial y^{g^*}}{\partial\boldsymbol{\alpha}^*}$$

$$\boldsymbol{L}_i=\left(\frac{\partial y^g}{\partial\boldsymbol{\sigma}}+\frac{\partial y_n^g}{\partial\boldsymbol{\chi}_n}\right)\Big/A_n;\quad \boldsymbol{L}^*=-\left(\frac{\partial y^g}{\partial\boldsymbol{\sigma}}+\frac{\partial y_n^g}{\partial\boldsymbol{\chi}_n}\right)\Big/A^*$$

After solving Eqs. $(35)_1$, $(35)_2$ and (32); estimating the nth non-negative multipliers in (33), and updating the internal variables using all the flow rules and the generalized stresses from Eqs. (17) and (28), we obtain a drift corrected incremental response for the modified framework.

4. A technique for modeling kinematic stiffness-regions

4.1. Experimental observations

It is widely accepted that in most types of continuous loading in soils the stiffness at small strains reduces rapidly, as indicated for example by Hardin and Drnevich (1972), Jardine (1992) and Smith et al. (1992). In order to capture this rapid reduction of stiffness, it is common to assume that the stress domain up to the large-scale yielding is divided into two or three sub-domains with different characterizations. Frequently, it is assumed that there exists a very small kinematic linear elastic nucleus in stress space, which is bounded by a yield surface referred to as Y1. However, as pointed out by Jardine (1992), it is difficult to locate this surface or even to prove its existence for most soils, maybe except for strongly cemented soils. The second domain (alternatively the first, if Y1 is ignored) is bounded by a second yield surface Y2, which marks the limit where reduction of stiffnesses becomes moderate, and is called the small strain region (SSR). The region between Y2 and the large-scale yielding surface Y3 is characterized as a domain of transition, where the plastic components of straining become ever larger as the stress point approaches the Y3 surface. The soil behavior inside Y3 is hysteretic. As already mentioned, at a certain instant (which in this scheme is described by encountering Y3) there is an abrupt yielding and the material undergoes larger plastic straining; frequently this is what soil models of conventional elastoplasticity refer to as yielding. The zone boundaries Y1, Y2 and Y3 are mobile and may change their shape and size as they follow the current stress point. A key feature of this experimental scheme is that up to Y3, the soil behavior could be characterized by kinematic translation of yield surfaces such that their location enables the material to 'remember' events in recent history.

In order to clarify how the kinematic hardening scheme works we will later provide an illustration for the particular CHCS model (see Section 6.4). But before that, we are going to establish the technique for utilizing the kinematic stiffness region scheme within the modified framework given in Section 3.

4.2. The new technique

Before presenting the CHCS model, it is important that we establish a technique for applying the kinematic stiffness region scheme. This is achieved by determining a one-dimensional model. As described by Puzrin and Houlsby (2001b) the continuous Iwan–Mroz model could be completely specified by two functionals; for example the Gibbs potential functional and the dissipation potential functional or alternatively the field of yield functions

$$\left.\begin{aligned} &g[\sigma,\hat{\alpha}] = -\tfrac{\sigma^2}{2E_0} - \sigma\varepsilon_{\mathrm{p}} + \tfrac{E_0}{2}\int_0^1 H(\eta)\hat{\alpha}(\eta)^2\,\mathrm{d}\eta \quad \text{and} \\ &d^g(\dot{\hat{\alpha}}) = \int_0^1 k\eta|\dot{\hat{\alpha}}(\eta)|\,\mathrm{d}\eta \geqslant 0 \quad \text{or} \\ &\hat{y}^g(\hat{\chi},\eta) = \hat{\chi}(\eta)^2 - k^2\eta^2 \leqslant 0 \quad \forall\eta\in\{0,1\} \end{aligned}\right\} \tag{36}$$

where $\varepsilon_{\mathrm{p}} = \int_0^1 \hat{\alpha}(\eta)\,\mathrm{d}\eta$ and the distribution function $H(\eta)$ is uniquely related to the second derivative of the initial back-bone curve $\varepsilon(\sigma)$, through

$$\frac{\partial^2\varepsilon}{\partial\sigma^2} = \frac{1}{kE_0H(\sigma/k)} \tag{37}$$

For example, it has been shown that the hyperbolic stress–strain curve $\varepsilon = \frac{k}{E_0}\frac{\sigma}{k-\sigma}$ is defined by utilizing $H(\eta) = (1-\eta)^3/2$.

Let us modify the Gibbs potential $(36)_1$, so that

$$g[\sigma,\hat{\alpha},\alpha^*] = -\frac{\sigma^2}{2E_0} - \sigma\varepsilon_{\mathrm{p}} + \frac{E_0}{2}\int_0^{\omega} H_0\Big(\frac{\eta}{\omega}\Big)\hat{\alpha}^2\,\mathrm{d}\eta + \frac{R_1E_0}{2}\int_{\omega}^1 H_1\Big(\frac{\eta-\omega}{1-\omega}\Big)\hat{\alpha}^2\,\mathrm{d}\eta \tag{38}$$

where R_1 and ω are parameters to be specified later and the form of (38) conforms to the general equation (9) in the unified framework, while $\varepsilon_{\mathrm{p}} = \int_0^1 \hat{\alpha}(\eta)\,\mathrm{d}\eta + \alpha^*$.

Next, let us update the dissipation in $(36)_2$ by

$$d^g[\alpha^*,\dot{\hat{\alpha}},\dot{\alpha}^*] = k\Pi(\alpha^*)\left\{\int_0^1 [\eta_{\mathrm{Y1}} + (1-\eta_{\mathrm{Y1}})\eta]|\dot{\hat{\alpha}}(\eta)|\,\mathrm{d}\eta + |\dot{\alpha}^*|\,\mathrm{d}\eta\right\} \geqslant 0 \tag{39}$$

where η_{Y1} represents the relative size of the elastic nucleus compared to Y3 (sized by the parameter k).

Note that the form of dissipation in (39) agrees with the general one in (5), whilst $\Pi(\alpha^*)$ is a positively defined hardening/softening function (in order that (39) will always be satisfied) that conforms to the boundary condition $\Pi(\alpha^*=0)\equiv 1$. This function leads to hardening when α^* increases and softening when its value decreases. It can be shown that the new dissipation alters the field of yield functions through Legendre transformation (14)

$$\hat{y}^g(\hat{\chi},\alpha^*,\eta) = \hat{\chi}(\eta)^2 - k^2[\eta_{\mathrm{Y1}} + (1-\eta_{\mathrm{Y1}})\eta]^2\Pi(\alpha^*)^2 \leqslant 0 \quad \forall\eta\in\{0,1\} \tag{40}$$

and through Legendre transformation (12) adds an additional isotropic hardening/softening yield function

$$y^{g^*}(\chi^*,\alpha^*) = (\chi^*)^2 - k^2\Pi(\alpha^*)^2 \leqslant 0 \tag{41}$$

The stress space expressions for these functions are found by implementing Eqs. (11) and (38)

$$\left.\begin{aligned} &\hat{y}^g_{\mathrm{T}}(\sigma,\alpha^*,\hat{\alpha},\eta) = [\sigma-\hat{\rho}(\hat{\alpha})]^2 - k^2[\eta_{\mathrm{Y1}} + (1-\eta_{\mathrm{Y1}})\eta]^2\Pi(\alpha^*)^2 \leqslant 0 \quad \forall\eta\in\{0,1\} \\ &y^{g^*}_{\mathrm{T}}(\sigma,\alpha^*) = \sigma^2 - k^2\Pi(\alpha^*)^2 \leqslant 0 \end{aligned}\right\} \tag{42}$$

where

$$\hat{\rho}(\hat{\alpha}) = \begin{cases} E_0H_0\big(\frac{\eta}{\omega}\big)\hat{\alpha} & \text{for } 0<\eta\leqslant\omega \\ E_0R_1H_1\big(\frac{\eta-\omega}{1-\omega}\big)\hat{\alpha} & \text{for } \omega\leqslant\eta\leqslant 1 \end{cases}$$

We see, then, that $\hat{\rho}(\hat{\alpha}=0)\equiv 0$ during initial conditions which implies that $\hat{y}^g_{\mathrm{T}}(\sigma,\alpha^*,\hat{\alpha},1) = y^{g^*}_{\mathrm{T}}(\sigma,\alpha^*)$. Since from Eqs. (40) and (41), we see that $\hat{y}^g(\hat{\chi}(1),\alpha^*,1)$ and $y^{g^*}(\chi^*,\alpha^*)$ have also the same coordinates, then as we mentioned in Section 3, $\hat{\alpha}(1)\equiv 0$, which means that continuity exists between $(42)_1$ and $(42)_2$; thus we always have

$$\hat{y}^g_{\mathrm{T}}(\sigma,\alpha^*,\hat{\alpha},1) \equiv \sigma^2 - k^2\Pi(\alpha^*)^2 \leqslant 0 \tag{43}$$

By examining the new setting, we identify a subdivision of the stress domain into four different stiffness zones.

Zone I. The size of the first zone (the elastic stress-space nucleus, bounded inside Y1) is configured by $\eta_{Y1}k\Pi(\alpha^*)$ (considering Eq. $(42)_1$ for $\eta = 0$). If the outer yield surface has not experienced any yielding, i.e. $\alpha^* = 0$, the size of the elastic nucleus is given by $\eta_{Y1}k$. This should be compared with the previous model (36) in which the stress-space nucleus of the elastic domain always shrinks to a point (in that case at $\sigma = 0$).

Zone II. The second zone governs the model's behavior whenever the largest active yield surface, such that $\hat{y}^g(\hat{\chi}(\bar{\eta}), \alpha^*, \bar{\eta}) = 0$, corresponds to $0 < \bar{\eta} \leqslant \omega$. In general, the size of Y2 is given from $(42)_1$ by $\eta_{Y2}k\Pi(\alpha^*) = [\eta_{Y1} + (1 - \eta_{Y1})\omega]k\Pi(\alpha^*)$, where ω is a parameter that defines the size of the Y2 yield surface, which bounds the domain. Its value is calculated by

$$\omega = \frac{\eta_{Y2} - \eta_{Y1}}{1 - \eta_{Y1}} \tag{44}$$

where η_{Y2} represents the relative size of Y2 compared to Y3. If, for example, we ignore the existence of the elastic nucleus, then $\eta_{Y1} = 0$ and $\omega = \eta_{Y2}$, such that ω also represents the relative size of Y2 compared to Y3.

The stiffness variation within this region is predetermined by the distribution function $H_0(\eta/\omega)$. This function should allow rapid reduction of the stiffness and ensure that at the end of the region, i.e. when $\bar{\eta} = \omega$, $H_0(1) = R_1$. We find, then, that R_1 is a parameter defining the amount of stiffness reduction in the transition from Y1 to Y2. The calibration of $H_0(\eta/\omega)$ is achieved by utilizing Eq. (37) as for the previous continuous Iwan–Mroz model, while the term η/ω maps the coordinate from zero to one, and replaces the previous dependency on η.

Zone III. The third zone controls the behavior whenever the largest active yield surface, such that $\hat{y}^g(\hat{\chi}(\bar{\eta}), \alpha^*, \bar{\eta}) = 0$, corresponds to $\omega \leqslant \bar{\eta} < 1$. As before, for the calibration of the distribution function $H_1(\frac{\eta-\omega}{1-\omega})$ we use Eq. (37), though this time $\frac{\eta-\omega}{1-\omega}$ maps the coordinate from zero to one. The initial stiffness of this zone is the same as the final stiffness of zone II, since $H_0(1)E_0 = R_1E_0$.

Zone IV. This zone is encountered whenever the single hyperplastic isotropic hardening yield function is reached, i.e. whenever $y_T^{g^*}(\chi^*, \alpha^*) = 0$. As mentioned before, the last surface in the continuous region, i.e. $\hat{y}_T^g(\sigma, \alpha^*, \hat{\alpha}, 1)$, yields simultaneously, but contributes no plastic flow (according to Section 3), since it coincides with the region's boundary Y3. The stiffness varies according to the hardening function $\Pi(\alpha^*)$ found in $(42)_2$ and (43), since $\sigma = k\Pi(\alpha^*)$. The tangential stiffness in this region is given by $\frac{\partial\sigma}{\partial\varepsilon} = \frac{\partial\sigma}{\partial\alpha^*} \cdot \frac{\partial\alpha^*}{\partial\varepsilon} = k\Pi'(\alpha^*)$. Since the only restriction on the value of parameter $R_2 = H_1(1)$, representing the stiffness reduction within the third zone, is to be greater than zero, there is principally an abrupt change in behavior at the first instant that Y3 yields, which supports the observation in Fig. 1. It can be seen that in Y3 two surfaces exist: one is an "active" surface $y_T^{g^*}$ and the other is a "passive" surface $\hat{y}_T^g$ for $\eta = 1$; this carries the memory for the abrupt change in Y3.

The presented approach provides a general idea of how the scheme of the stiffness regions can be incorporated within the framework described in Section 2. However, at this stage, the model has been one-dimensional only, and the functions $\Pi(\alpha^*)$, $H_0(\eta/\omega)$ and $H_1(\frac{\eta-\omega}{1-\omega})$ have yet to be determined.

4.3. Distribution functions

It has been shown elsewhere (for example Jardine et al., 1986; Burland, 1989) that in many geotechnical soil–structure interaction problems stiffness reduction within the SSR is very important. This is why when defining the distribution functions we focus mainly on the behavior within the SSR, without neglecting the accuracy of prediction at the larger strains.

As we indicated before, the first distribution function $H_0(\eta)$ should satisfy the following boundary condition $H_0(1) = R_1$. However, the function should also describe the substantial reduction in stiffness

inside the SSR. A possible alternative is given by the normalized Ramberg–Osgood power function (see Ramberg and Osgood, 1943)

$$x = y + ay^r \quad \text{for } 0 \leqslant x \leqslant x_L \text{ and } 0 \leqslant y \leqslant 1 \tag{45}$$

where $y = \sigma/k; x = E_0\varepsilon/k; x_L = E_0\varepsilon_L/k$ and a and r are parameters chosen to ensure that the conditions (a) $x(y=0) \equiv 0$; (b) $\mathrm{d}x/\mathrm{d}y(y=0) \equiv 1$; (c) $x(y=1) \equiv x_L$; (d) $\mathrm{d}x/\mathrm{d}y(y=1) \equiv 1/R_1$; (e) $\mathrm{d}x/\mathrm{d}y > 0$ and $\mathrm{d}^2x/\mathrm{d}y^2 > 0$, are satisfied, so that

$$a = x_L - 1; \quad r = \frac{1 - R_1}{R_1 a} \tag{46}$$

As is seen from Eq. (37), in order to define the distribution function $H_0(\eta)$,the second derivatives $\partial^2\varepsilon/\partial\sigma^2$ of (45) are required. Since $\frac{\partial\varepsilon}{\partial\sigma} = \frac{\partial\varepsilon}{\partial x}\frac{\partial x}{\partial y}\frac{\partial y}{\partial\sigma}$, $x = E_0\varepsilon/k$ and $y = \sigma/k$ we obtain

$$\frac{\partial^2\varepsilon}{\partial\sigma^2} = \frac{1}{kE_0}\frac{\partial^2 x}{\partial y^2} \tag{47}$$

From combining Eqs. (37), (45) and (47) it follows that $H_0(\eta) = \eta^{2-r}/\alpha r(r-1)$ is a very convenient form. As already mentioned, this function is only appropriate for the continuous Iwan–Mroz model (Eq. (36)), and in order to adjust it to the stress–strain behavior in Zone II, we use

$$H_0(\eta/\omega) = \frac{(\eta/\omega)^{2-r}}{\alpha r(r-1)} \tag{48}$$

Within Zone III, the requirement for prediction accuracy is less strict and, hence, the function can satisfy fewer geometrical conditions and involve fewer parameters. The stiffness reduction is moderate and can be described, for example, by a simple normalized hyperbolic function (Kondner, 1963): $x = y/(1-y)$. However, unlike this function, it should not allow failure, and a finite stiffness condition should be met. The following modified hyperbolic function can be:

$$x = \frac{y}{1 - by} \quad \text{for } 0 \leqslant y \leqslant 1 \tag{49}$$

that satisfies the conditions (a) $x(y=0) \equiv 0$; (b) $\mathrm{d}x/\mathrm{d}y(y=0) \equiv 1$; (c) $x(y=1) \equiv x_L$; (d) $\mathrm{d}x/\mathrm{d}y > 0$ and $\mathrm{d}^2x/\mathrm{d}y^2 > 0$, then

$$b = \frac{x_L - 1}{x_L} \tag{50}$$

where compared to the Ramberg–Osgood function we drop the restricting condition on $\mathrm{d}x/\mathrm{d}y$ at $y = 1$.

From combining Eqs. (37), (49) and (47) it follows that $H_1(\eta) = (1 - b\eta)^3/2b$. In order to adjust it to the stress–strain behavior in Zone III, we shall use

$$H_1\left(\frac{\eta - \omega}{1 - \omega}\right) = \left(1 - b\frac{\eta - \omega}{1 - \omega}\right)^3 \Big/ 2b \tag{51}$$

In Fig. 2 we present a comparison between the two normalized functions (in Eqs. (45) and (49)). Fig. 2a presents their normalized stress–strain curve. Both functions satisfy the initial stiffness (dashed line), final strain and final stress conditions, though only the Ramberg–Osgood function satisfies the finite stiffness requirement (another dashed line). This is the reason why the stiffness reduction by the Ramberg–Osgood function in Fig. 2b is more pronounced, which is of main concern inside the SSR. However, both result in conceptually "S-shaped" curves of secant shear stiffness against the logarithm of shear strain as observed for soils, which may justify the use of the modified hyperbolic beyond the SSR.

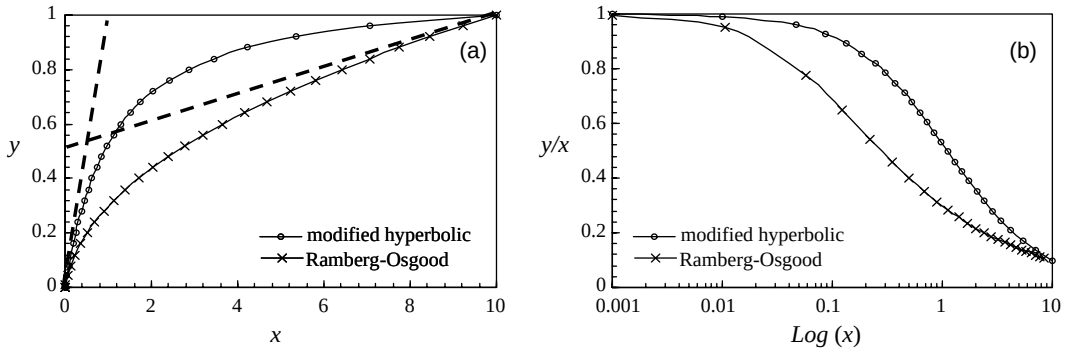

Fig. 2. Comparison between the Ramberg–Osgood and modified hyperbolic functions.

5. Definition of CHCS model

As previously indicated, the two energy potential functionals (5) and (9) define a unified continuous hyperplastic model with an additional isotropic hardening/softening hyperplastic surface. In this section we extend the technique given in Section 4 for a two dimensional model using the triaxial stress and strain variables.

5.1. Definition of triaxial variables

Let us denote stresses by $\vec{\mathbf{A}} = \{\boldsymbol{\sigma}, \hat{\boldsymbol{\chi}}, \hat{\bar{\boldsymbol{\chi}}}, \boldsymbol{\chi}^*, \bar{\boldsymbol{\chi}}^*\}$, then the stress-like triaxial variables are defined using

$$\vec{P} = \frac{1}{3}\vec{\mathbf{A}} : \mathbf{1}, \quad \vec{Q} = \sqrt{\frac{3}{2}\vec{\boldsymbol{\Theta}} : \vec{\boldsymbol{\Theta}}}, \quad \vec{\boldsymbol{\Theta}} = \vec{\mathbf{A}} - \vec{P}\mathbf{1} \tag{52}$$

where $\vec{P} = \{p, \hat{\chi}_p, \hat{\bar{\chi}}_p, \chi_p^*, \bar{\chi}_p^*\}$ and $\vec{Q} = \{q, \hat{\chi}_q, \hat{\bar{\chi}}_q, \chi_q^*, \bar{\chi}_q^*\}$, respectively, denote the vector of mean and deviatoric stresses. If we also unify strain-like variables by $\vec{\mathbf{B}} = \{\boldsymbol{\varepsilon}, \hat{\boldsymbol{\alpha}}, \boldsymbol{\alpha}^*\}$, then the strain-like triaxial variables are given by

$$\vec{V} = \vec{\mathbf{B}} : \mathbf{1}, \quad \vec{S} = \sqrt{\frac{2}{3}\vec{\boldsymbol{\gamma}} : \vec{\boldsymbol{\gamma}}}, \quad \vec{\boldsymbol{\gamma}} = \vec{\mathbf{B}} - \frac{1}{3}\vec{V}\mathbf{1} \tag{53}$$

where $\vec{V} = \{\varepsilon_{\mathrm{v}}, \hat{\alpha}_{\mathrm{v}}, \alpha_{\mathrm{v}}^*\}$ and $\vec{S} = \{\varepsilon_{\mathrm{s}}, \hat{\alpha}_{\mathrm{s}}, \alpha_{\mathrm{s}}^*\}$ correspondingly denote the vector of volumetric and shear strains. In the above, $\mathbf{1}$ is the second-order identity tensor, where $(\mathbf{1})_{ij} = \delta_{ij}$ is the Kronecker delta.

5.2. Definition of Gibbs free-energy functional

The first energy potential functional is the Gibbs free energy

$$g(\boldsymbol{\sigma}, \hat{\boldsymbol{\alpha}}, \boldsymbol{\alpha}^*) = g_1(\boldsymbol{\sigma}) + g_2(\hat{\boldsymbol{\alpha}}) - \left\{ \int_0^1 \hat{\alpha}_{\mathrm{v}}(p - (1-\eta_{\mathrm{Y1}})(1-\eta)p_0)\,\mathrm{d}\eta + \int_0^1 \hat{\alpha}_{\mathrm{s}}(q - (1-\eta_{\mathrm{Y1}})(1-\eta)q_0)\,\mathrm{d}\eta \right\} - p\alpha_{\mathrm{v}}^* - q\alpha_{\mathrm{s}}^* \tag{54}$$

where

$$g_1(\boldsymbol{\sigma}) = -\frac{p^{2-m} - (2-m)p \cdot p_0^{1-m}}{\bar{K}(2-m)(1-m)p_r^{1-m}} - \frac{q^2}{6\bar{G}p_r^{1-n}p^n} + \frac{q_0(2qp_0 - nq_0p)}{6\bar{G}p_r^{1-n}p_0^{1+n}} + \frac{(p-p_0)(q-q_0)}{J_0} \tag{55}$$

for any m, apart from when $m = 1$, in which case taking the limit of Eq. (55) gives

$$g_1(\boldsymbol{\sigma}) = -\kappa^* p\left(L_n\left[\frac{p}{p_0}\right] - 1\right) - \frac{q^2}{6\bar{G}p_r^{1-n}p^n} + \frac{q_0(2q - q_0 p_n)}{6\bar{G}p_r^{1-n}p_0^n} + \frac{(p-p_0)(q-q_0)}{J_0} \tag{56}$$

The first component $g_1(\boldsymbol{\sigma})$ (in either (55) or (56) is the hyperelastic Gibbs potential proposed by Einav and Puzrin (2003a), except for the last term $(p-p_0)(q-q_0)/J_0$. This term is added to account for the inherent anisotropy of the material, whilst J_0 is the inherent anisotropy modulus parameter. While $g_1(\boldsymbol{\sigma})$ describes the energy potential component that controls the hyperelastic behavior of the model,

$$\begin{aligned} g_2(\hat{\boldsymbol{\alpha}}) = &\int_0^{\omega}\left[H_0^K\left(\frac{\eta}{\omega}\right)\frac{K_0\hat{\alpha}_{\mathrm{v}}^2}{2} + H_0^G\left(\frac{\eta}{\omega}\right)\frac{3G_0\hat{\alpha}_{\mathrm{s}}^2}{2}\right]\mathrm{d}\eta \\ &+ R_1\int_{\omega}^{1}\left[H_1^K\left(\frac{\eta-\omega}{1-\omega}\right)\frac{K_0\hat{\alpha}_{\mathrm{v}}^2}{2} + H_1^G\left(\frac{\eta-\omega}{1-\omega}\right)\frac{3G_0\hat{\alpha}_{\mathrm{s}}^2}{2}\right]\mathrm{d}\eta \end{aligned} \tag{57}$$

is the component that defines the kinematic hardening nature of the model. Since the amount of stiffness reduction and the accompanying strain in the deviatoric and volumetric directions are normally different, we will use two separate distribution functions. Their format is the same, but their parameters are different.

In principle, the use of non-linear elasticity (55) instead of linear elasticity as configured in the one-dimensional case (see Eq. $(36)_1$), should require certain modification of the stress-strain backbone curve expression. However, the corresponding calibration of the functions results in unnecessary complications that will result in expressions which are difficult to extract.

5.3. Definition of dissipation functional

The second potential functional is the dissipation

$$d^g(\dot{\hat{\boldsymbol{\alpha}}}, \dot{\boldsymbol{\alpha}}^*, \boldsymbol{\alpha}^*, \eta) = \frac{p_{y0}\Pi(\boldsymbol{\alpha}^*)}{2}\left\{\int_0^1 [\eta_{\mathrm{Y1}} + (1-\eta_{\mathrm{Y1}})\eta]\left(\sqrt{\dot{\hat{\alpha}}_{\mathrm{v}}^2 + M^2\dot{\hat{\alpha}}_{\mathrm{s}}^2} + \dot{\hat{\alpha}}_{\mathrm{v}}\right)\mathrm{d}\eta + \left(\sqrt{(\dot{\alpha}_{\mathrm{v}}^*)^2 + M^2(\dot{\alpha}_{\mathrm{s}}^*)^2} + \dot{\alpha}_{\mathrm{v}}^*\right)\right\} \geqslant 0 \tag{58}$$

where M is the slope of the residual strength criterion; p_{y0} is the initial pre-consolidation pressure and

$$\Pi(\boldsymbol{\alpha}^*) = \exp(\alpha_{\mathrm{v}}^*/\lambda^* - \kappa^*) \tag{59}$$

is a positively defined hardening/softening function, satisfying the boundary condition $\Pi(\boldsymbol{\alpha}^* = 0) \equiv 1$, where λ^* and κ^* are the slope of the virgin compression line (VCL) and the initial slope of the swelling line in $(\ln(V), \ln(p))$ space. Note that the parameter κ^* is not an extra parameter, since for the case $m = 1$ it is directly specified by Eq. (56), and indirectly defined through Eq. (55) for any other value of m.

6. Functional interpretation

6.1. The CHCS field of yield surfaces

The dissipative generalized stresses in Eq. (6) are given by

$$\hat{\chi}_p = \frac{\partial d}{\partial \dot{\hat{\alpha}}_{\mathrm{v}}} = \frac{p_{y0}\Pi(\boldsymbol{\alpha}^*)}{2}\left\{[\eta_{\mathrm{Y1}} + (1-\eta_{\mathrm{Y1}})\eta]\left(\frac{M^2\dot{\hat{\alpha}}_{\mathrm{v}}}{\sqrt{\dot{\hat{\alpha}}_{\mathrm{v}}^2 + M^2\dot{\hat{\alpha}}_{\mathrm{s}}^2}} + 1\right)\right\} \tag{60}$$

$$\hat{\chi}_q = \frac{\partial d}{\partial \dot{\hat{\alpha}}_s} = \frac{p_{y0}\Pi(\boldsymbol{\alpha}^*)}{2}[\eta_{Y1} + (1-\eta_{Y1})\eta]\frac{M^2\dot{\hat{\alpha}}_s}{\sqrt{\dot{\hat{\alpha}}_v^2 + M^2\dot{\hat{\alpha}}_s^2}} \tag{61}$$

and

$$\chi_p^* = \frac{\partial d}{\partial \dot{\alpha}_v^*} = \frac{p_{y0}\Pi(\boldsymbol{\alpha}^*)}{2}\left(\frac{\dot{\alpha}_v^*}{\sqrt{(\dot{\alpha}_v^*)^2 + M^2(\dot{\alpha}_s^*)^2}} + 1\right) \tag{62}$$

$$\chi_q^* = \frac{\partial d}{\partial \dot{\alpha}_s^*} = \frac{p_{y0}\Pi(\boldsymbol{\alpha}^*)}{2}\frac{M^2\dot{\alpha}_s^*}{\sqrt{(\dot{\alpha}_v^*)^2 + M^2(\dot{\alpha}_s^*)^2}} \tag{63}$$

By changing the position of the last terms in (60) to the left-hand side, squaring Eqs. (60) and (61), adding them together and rearranging the terms, we derive the field of yield functions

$$\hat{y}(\hat{\boldsymbol{\chi}}, \boldsymbol{\alpha}^*, \eta) = \left(\hat{\chi}_p - [\eta_{Y1} + (1-\eta_{Y1})\eta]\frac{p_{y0}\Pi(\alpha^*)}{2}\right)^2 + \left(\frac{\hat{\chi}_q}{M}\right)^2 - \left(\frac{p_{y0}\Pi(\alpha^*)}{2}[\eta_{Y1} + (1-\eta_{Y1})\eta]\right)^2 \leqslant 0 \tag{64}$$

Then, by repeating this procedure for (62) and (63), we get the outer yield function (Y3)

$$y^{g^*}(\boldsymbol{\chi}^*, \boldsymbol{\alpha}^*) = \left(\chi_p^* - \frac{p_{y0}\Pi(\boldsymbol{\alpha}^*)}{2}\right)^2 + \left(\frac{\chi_q^*}{M}\right)^2 - \left(\frac{p_{y0}\Pi(\boldsymbol{\alpha}^*)}{2}\right)^2 \leqslant 0 \tag{65}$$

where we note that in the generalized stress space, the Y3 yield surface coincides with the largest yield surface given by Eq. (64), since $\hat{y}(\hat{\boldsymbol{\chi}}(1), \boldsymbol{\alpha}^*, \eta = 1) = y^{g^*}(\hat{\boldsymbol{\chi}}^*, \boldsymbol{\alpha}^*)$.

6.2. The CHCS hyperelastic component

Differentiating the Gibbs free energy (54) by p and q yields the volumetric strains

$$\varepsilon_v = -\frac{\partial g}{\partial p} = \frac{p^{1-m} - p_0^{1-m}}{\bar{K}(1-m)p_r^{1-m}} - \frac{nq^2}{6\bar{G}p_r^{1-n}p^{1+n}} + \frac{nq_0^2}{6\bar{G}p_r^{1-n}p_0^{1+n}} - \frac{q-q_0}{J_0} + \int_0^1 \hat{\alpha}_v \,\mathrm{d}\eta + \alpha_v^* \tag{66}$$

apart from when $m = 1$, in which case

$$\varepsilon_v = -\frac{\partial g}{\partial p} = \kappa^* L_n\left[\frac{p}{p_0}\right] - \frac{nq^2}{6\bar{G}p_r^{1-n}p^{1+n}} + \frac{nq_0^2}{6\bar{G}p_r^{1-n}p_0^{1+n}} - \frac{q-q_0}{J_0} + \int_0^1 \hat{\alpha}_v \,\mathrm{d}\eta + \alpha_v^* \tag{67}$$

and shear strain

$$\varepsilon_s = -\frac{\partial g}{\partial q} = \frac{q}{3\bar{G}p_r^{1-n}p^n} - \frac{q_0}{3\bar{G}p_r^{1-n}p_0^n} - \frac{p-p_0}{J_0} + \int_0^1 \hat{\alpha}_s \,\mathrm{d}\eta + \alpha_s^* \tag{68}$$

where $(\int_0^1 \hat{\alpha}_v \,\mathrm{d}\eta + \alpha_v^*)$ and $(\int_0^1 \hat{\alpha}_s \,\mathrm{d}\eta + \alpha_s^*)$ are identified as the volumetric and shear plastic strains. Both of these expressions are consistent in giving zero elastic strains for initial conditions ($p = p_0$ and $q = q_0$).

Differentiating the volumetric and shear strains in Eqs. (66) and (68) with respect to p and q produces the hyperelastic compliance matrix

$$C = \begin{bmatrix} \dfrac{-\partial^2 g_1}{\partial p^2} & \dfrac{-\partial^2 g_1}{\partial p \partial q} \\ \dfrac{-\partial^2 g_1}{\partial q \partial p} & \dfrac{-\partial^2 g_1}{\partial q^2} \end{bmatrix} = \begin{bmatrix} \dfrac{1}{\bar{K} p_r (p/p_r)^m} + \dfrac{\bar{n}\Omega^2}{3\bar{G} p_r (p/p_r)^n} & -\dfrac{n\Omega}{3\bar{G} p_r (p/p_r)^n} - \dfrac{1}{J_0} \\ -\dfrac{n\Omega}{3\bar{G} p_r (p/p_r)^n} - \dfrac{1}{J_0} & \dfrac{1}{3\bar{G} p_r (p/p_r)^n} \end{bmatrix} \tag{69}$$

where $\Omega = q/p$ is the stress ratio, and $\bar{n} = n(n+1)/2$. Differentiating (67) and (68) gives

$$C = \begin{bmatrix} \dfrac{\kappa^*}{p} + \dfrac{\bar{n}\Omega^2}{3\bar{G} p_r (p/p_r)^n} & -\dfrac{n\Omega}{3\bar{G} p_r (p/p_r)^n} - \dfrac{1}{J_0} \\ -\dfrac{n\Omega}{3\bar{G} p_r (p/p_r)^n} - \dfrac{1}{J_0} & \dfrac{1}{3\bar{G} p_r (p/p_r)^n} \end{bmatrix}$$

is consistent to Eq. (69) for $m = 1$.

This compliance matrix degenerates into the one given in Einav and Puzrin (2003a), when the absolute of inherent anisotropy parameter $|J_0|$ approaches infinity. As $|J_0|$ becomes smaller the amount of inherent anisotropy tends to grow. The sign of J_0 determines the direction in which the material is anisotropic due to its previous mode of loading. A positive sign corresponds to inherent horizontal tixotropy, as commonly observed in post-glacial clays. The apparent elastic bulk and shear moduli are, respectively, given by

$$K'(p) = \bar{K} p_r (p/p_r)^m, \quad G'(p) = \bar{G} p_r (p/p_r)^n \tag{70}$$

which defines the constants K_0 and G_0 ($K'(p_0)$ and $G'(p_0)$, respectively) used in the second part of the Gibbs potential function (57).

6.3. Translation rules

The translation rule for the yield surfaces depends on the zone to which zone each surface.

Zone I. In this zone, dissipation does not occur and the model behaves purely as hyperelastic material and no translation is experienced.

Zone II. The isotropic and deviatoric components of the generalized stresses are given by Eqs. $(8)_1$ and (54); for this zone $0 < \eta \leqslant \omega$, thus

$$\hat{\tilde{\chi}}_p = -\frac{\partial g}{\partial \hat{\alpha}_v} = p - (1 - \eta_{Y1})(1 - \eta) p_0 - H_0^K \left(\frac{\eta}{\omega}\right) K_0 \hat{\alpha}_v \tag{71}$$

$$\hat{\tilde{\chi}}_q = -\frac{\partial g}{\partial \hat{\alpha}_s} = q - (1 - \eta_{Y1})(1 - \eta) q_0 - 3H_0^G \left(\frac{\eta}{\omega}\right) G_0 \hat{\alpha}_s \tag{72}$$

By applying Ziegler's orthogonality principle in the form $\{\hat{\tilde{\chi}}_p, \hat{\tilde{\chi}}_q\} = \{\hat{\chi}_p, \hat{\chi}_q\}\ \forall \eta \in \{0, 1\}$ the back stress function can be expressed according to $(11)_1$ and (57), which after differentiation yields the translation rule for the field of yield surfaces

$$\dot{\hat{\rho}}_p = \frac{\partial^2 g_2}{\partial \hat{\alpha}_v^2} \dot{\hat{\alpha}}_v = \dot{p} - \dot{\hat{\tilde{\chi}}}_p = H_0^K \left(\frac{\eta}{\omega}\right) K_0 \dot{\hat{\alpha}}_v \tag{73}$$

$$\dot{\hat{\rho}}_q = \frac{\partial^2 g_2}{\partial \hat{\alpha}_s^2} \dot{\hat{\alpha}}_s = \dot{q} - \dot{\hat{\tilde{\chi}}}_q = 3H_0^G \left(\frac{\eta}{\omega}\right) G_0 \dot{\hat{\alpha}}_s \tag{74}$$

Zone III. For this zone $\omega \leqslant \eta \leqslant 1$, thus

$$\hat{\tilde{\chi}}_p = -\frac{\partial g}{\partial \hat{\alpha}_v} = p - (1 - \eta_{Y1})(1 - \eta) p_0 - R_1^K H_1^K \left(\frac{\eta - \omega}{1 - \omega}\right) K_0 \hat{\alpha}_v \tag{75}$$

$$\hat{\vec{\chi}}_q = -\frac{\partial g}{\partial \hat{\alpha}_s} = q - (1-\eta_{Y1})(1-\eta)q_0 - 3R_1^G H_1^G\left(\frac{\eta-\omega}{1-\omega}\right)G_0\hat{\alpha}_s \tag{76}$$

and the translation rule is given by

$$\dot{\hat{\rho}}_p = \frac{\partial^2 g_2}{\partial \hat{\alpha}_v^2}\dot{\hat{\alpha}}_v = \dot{p} - \dot{\hat{\chi}}_p = R_1^K H_1^K\left(\frac{\eta-\omega}{1-\omega}\right)K_0\dot{\hat{\alpha}}_v \tag{77}$$

$$\dot{\hat{\rho}}_q = \frac{\partial^2 g_2}{\partial \hat{\alpha}_s^2}\dot{\hat{\alpha}}_s = \dot{q} - \dot{\hat{\chi}}_q = 3R_1^G H_1^G\left(\frac{\eta-\omega}{1-\omega}\right)G_0\dot{\hat{\alpha}}_s \tag{78}$$

This resembles to the translation rule of the second zone, but using a different distribution function and the constant parameters R_1^K and R_1^G, which carry memory from the first distribution function.

Zone IV. This zone corresponds to the isotropic hardening/softening hyperplastic component of the model and to the yield surface y^{g^*}, thus

$$\vec{\chi}_p^* = -\frac{\partial g}{\partial \alpha_v^*} = p \tag{79}$$

$$\vec{\chi}_q^* = -\frac{\partial g}{\partial \alpha_s^*} = q \tag{80}$$

This yield surface does not translate since

$$\dot{\rho}_p^* = \frac{\partial^2 g}{\partial \alpha_v^{*2}}\dot{\alpha}_v^* = \dot{p} - \dot{\chi}_p^* = 0 \tag{81}$$

$$\dot{\rho}_q^* = \frac{\partial^2 g}{\partial \alpha_s^{*2}}\dot{\alpha}_s^* = \dot{q} - \dot{\chi}_q^* = 0 \tag{82}$$

meaning that no change of back stress is allowed.

6.4. Geometric interpretation of the yield surfaces

The form of the large-scale yield function y^{g^*} in true stress-space space is obtained by substituting the generalized stresses (Eqs. (79) and (80)) into the generalized yield function (65) (noting the Ziegler orthogonality condition)

$$y^{g^*}(\boldsymbol{\sigma}, \boldsymbol{\alpha}^*) = \left(p - \frac{p_{y0}\Pi(\boldsymbol{\alpha}^*)}{2}\right)^2 + \left(\frac{q}{M}\right)^2 - \left(\frac{p_{y0}\Pi(\boldsymbol{\alpha}^*)}{2}\right)^2 \leqslant 0 \tag{83}$$

which is analogous to the conventional plasticity MCC yield function. However, the largest yield function of the continuous hyperplastic field in (64) (i.e. when using $\eta = 1$) should have the same MCC expression in true stress space to guarantee continuity. In this case the generalized stresses given by Eqs. (75) and (76) take the form

$$\hat{\chi}_p(1) = p - R_1^K H_1^K(1)K_0\hat{\alpha}_v(1) = p - R_1^K R_2^K K_0\hat{\alpha}_v(1) \tag{84}$$

$$\hat{\chi}_q(1) = q - 3R_1^G H_1^G(1)G_0\hat{\alpha}_s(1) = q - 3R_1^G R_2^G G_0\hat{\alpha}_s(1) \tag{85}$$

By substituting (84) and (85) into the yield surface (64), for the case $\eta = 1$, we obtain the largest yield function in true stress space

$$\hat{y}(\boldsymbol{\sigma},\boldsymbol{\alpha}^*,1)=\left(p-\frac{p_{y0}\Pi(\boldsymbol{\alpha}^*)}{2}-R_1^K R_2^K K_0\hat{\alpha}_{\mathrm{v}}(1)\right)^2+\left(\frac{q-3R_1^G R_2^G G_0\hat{\alpha}_{\mathrm{s}}(1)}{M}\right)^2-\left(\frac{p_{y0}\Pi(\boldsymbol{\alpha}^*)}{2}\right)^2\leqslant 0 \tag{86}$$

This yield function agrees with (83) during initial conditions, since that according to Section 3, $\hat{\boldsymbol{\alpha}}(1)\equiv\mathbf{0}$ always, thus Eq. (86) could always be simplified by

$$\hat{y}(\boldsymbol{\sigma},\boldsymbol{\alpha}^*,1)=\left(p-\frac{p_{y0}\Pi(\boldsymbol{\alpha}^*)}{2}\right)^2+\left(\frac{q}{M}\right)^2-\left(\frac{p_{y0}\Pi(\boldsymbol{\alpha}^*)}{2}\right)^2\leqslant 0 \tag{87}$$

hence we have full similarity with (83), such that continuity between the surfaces exists. We see, then, that the kinematic nature of the last yield surface in the continuous field is not realized and only isotropic hardening of the surface occurs in order to guarantee consistency. As the continuous hyperplastic yield surfaces correspond to a smaller η, the constraining effect is reduced because the influence of λ^* on the value of $\hat{\lambda}(\eta)$ gets smaller. The important result here is that the failure criterion is governed by the outer yield surface, and not by the field of yield surfaces. This ensures compatibility with the single surface MCC model.

In Fig. 3(a)–(c) we schematically present the field of yield surfaces in true and generalized stress spaces for different phases of the loading process. The field of yield surfaces in true stress space is depicted in Fig. 3(a.1) for the initial state such that $p_y=p_{y0}$ and all internal variables are zero. In this space, the initial stress point is marked by $I=I(p_0,q_0)$. The bold ellipses Y1, Y2, and Y3 represent the elastic nucleus; the bounds of the SSR, and the large scale MCC yield surfaces respectively. Unlike Y1 and Y3, the mathematical definition of Y2 does not come from the dissipation, but from splitting the integral in the kinematic hardening component of the energy potential in (57) into two parts by the use of the parameter ω; a parameter that as already mentioned indicates the relative size of Y2 compared to Y1 and Y3 according to Eq. (44). In other words, the yield surface that corresponds to Y2 is the one satisfying η equals ω.

Fig. 3(a.2) also depicts the field of yield surfaces at initial conditions, but in the generalized stress space. The yield surfaces in this space always pass through the axis origin and form a continuous picture of the infinite field of generalized stress-space MCC yield surfaces. Each yield surface is the boundary of the generalized stress domain for the corresponding generalized stress point, as indicated in the scheme by the corresponding arrow. Considering Eqs. (71), (72), (75), (76), (79) and (80) we find that the initial points in that space lie on a vector $I^{\chi(\eta)}\{\hat{\chi}_p^0,\hat{\chi}_q^0\}=[\eta+(1-\eta)\eta_{\mathrm{Y1}}]I(p_0,q_0)$, connecting point $I^{\chi(0)}=\eta_{\mathrm{Y1}}I(p_0,q_0)$, related to Y1, and point $I^{\chi(1)}=I^{\chi^*}=I(p_0,q_0)$, related to Y3. If we ignore the existence of the elastic nucleus, Y1 shrinks to a point and $\eta_{\mathrm{Y1}}=0$; the vector connecting the initial points becomes $I^{\chi(\eta)}=\eta I(p_0,q_0)$, which is the straight line connecting the axis origin to the true stress point.

Fig. 3(b.1) and (b.2) correspond to the field of yield surfaces after an arbitrary stress path I–F was followed. This stress path is depicted by a dashed curved line in the true stress space (Fig. 3(b.1)). In this particular example the stress path initially hits and drags all yield surfaces including Y3. Since y^{g^*} hardens isotropically, the pre-consolidation pressure grows and becomes $p_y=p_{y0}\Pi(\boldsymbol{\alpha}^*)$. As the stress path continues, it initially returns back inside Y1, Y2 and Y3 and later hits and drags Y1 and Y2 again, until it settles in zone III (on a final point which is indicated by $F(p_{\mathrm{f}},q_{\mathrm{f}})$. Prior to this loading all the initial generalized stress points are located on the same straight line (Fig. 3(a.2)); however, after implementing the stress path I–F, their positions deviate from the straight line (Fig. 3(b.2)). In this space, each yield surface behaves as an individual conventional MCC surface, without kinematic hardening, but with isotropic hardening/softening according to the function $\Pi(\boldsymbol{\alpha}^*)$ of the outer hyperplastic isotropic surface.

Note also that according to continuous hyperplasticity, the yield surfaces can intersect one another (see Puzrin and Houlsby, 2001c), which is consistent with the thermodynamics. Each generalized stress tensor, which is denoted in Fig. 3(b.2) by a point, relates to a corresponding yield surface (see Eqs. (64) and (65)) indicated by an arrow. When the point is on the surface, no arrow is shown.

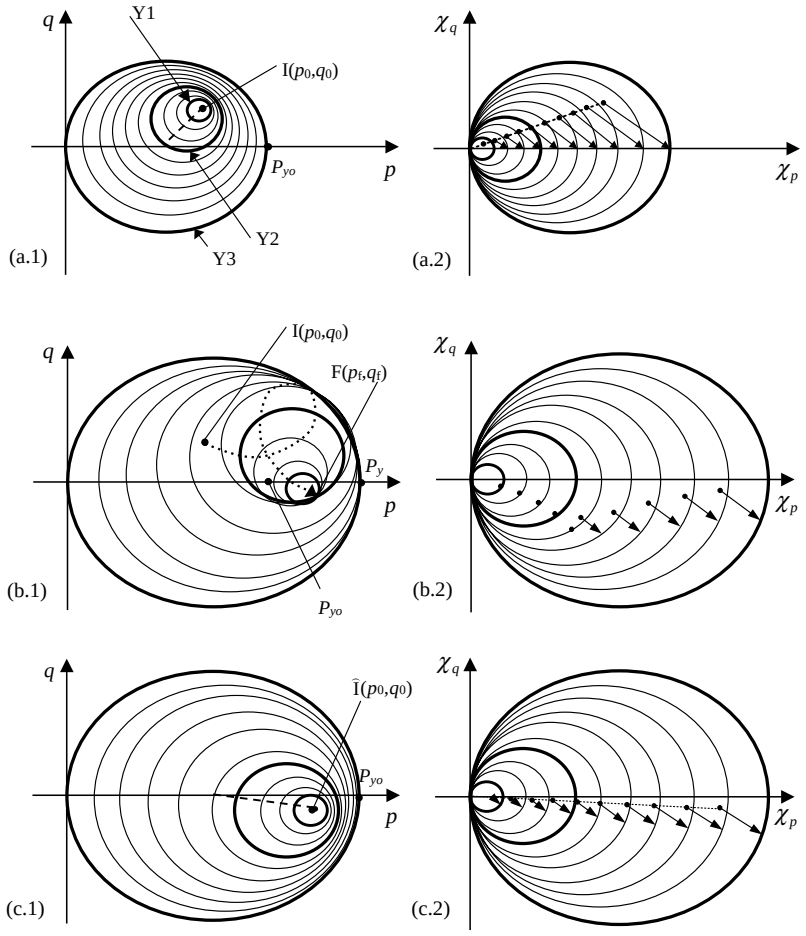

Fig. 3. Schematic geometric representation of yield surfaces in true and generalizes stress-spaces: (a) at initial conditions; (b) after quasi-static loading according to the *I–F* stress-path and (c) new initial conditions.

6.5. Assumption of initial positions of yield surfaces

In the CHCS model it is assumed that, if after a loading process the current stresses are maintained for sufficient period of time, the stiffness will locally increase after the loading is resumed again. This assumption is simulated in this model by centering the yield surfaces in a linear order on a line connecting the center of the large-scale yield surface with the required new initial stress state (Fig. 3(c.1)). The final stress point for the previous loading process becomes the initial point for the new process

$$F(p_{\mathrm{f}}, q_{\mathrm{f}}) = \widehat{I}(p_0, q_0)$$

where the superimposed hat on the '*I*' is added to indicate this is a new initial stress point.

The generalized yield surfaces do not experience any translation during the rearrangement process; however, we assume that the final points before the process commenced $F^{\chi(\eta)}$, shift toward the vector $\widehat{I}^{\chi(\eta)}$ (Fig. 2(c.2))

$$F^{\chi(\eta)}\{\hat{\chi}_p^f, \hat{\chi}_q^f\} \underset{\substack{\text{Complete}\\ \text{Ageing}}}{\rightarrow} \widehat{I}^{\chi(\eta)}\{\hat{\chi}_p^0, \hat{\chi}_q^0\} = [\eta + (1-\eta)\eta_{Y1}]\widehat{I}(p_0, q_0)$$

Note that while in stress space the point is fixed and the yield surfaces move, in generalized space the points move and the yield surfaces are fixed.

Needless to say, the above assumption requires more attention in the future research. The process of ageing is linked to mechanical evolution at the microstructure scale and to chemical processes. At the macroscopic level, the memory of these processes is probably reflected in changes in the values of the internal variables. The assumption that these changes cause the yield surfaces to be rearranged according to the above law requires further experimental verification.

7. Extension of the model to general stress space

The original framework of the MCC is based, almost exclusively, on laboratory results from conventional triaxial tests. The portions of stress space in which these tests operate are severely restricted, because the intermediate principal stress must be equal to either the major or minor principal stress. Experimental evidence reveals that the drained strength parameters vary depending on whether the material is subjected to triaxial compression or extension. The difference between these two types of test is that in the compression tests the intermediate principal stress, σ_2, is equal to the minor principal stress, σ_3, and the major principal stress, σ_1, is vertical. By contrast, in extension tests $\sigma_2 = \sigma_1$, and the latter stress acts horizontally. Obviously, these show only two extreme cases. At this stage position, the CHCS model suggests that the residual strength is the same for any loading direction (as in the extended von Mises material), since the projections of the yield surfaces are circular in the octahedral plane. To account for the more realistic strength dependency on the rotation of principal stress directions, the shape of the projection of the yield surfaces should be a function of the third stress invariant. An alternative is to use the family of plane yield surfaces proposed by van Eekelen (1980). The shape of the surfaces is governed by the parameters ξ, ψ and ς, and in the context of our work, this family is implemented by modifying the parameter M in the yield surface expressions (64) and (65)

$$M(\hat{\boldsymbol{\chi}}) = \xi \cdot (1 + \psi \mathrm{Sin}(3\hat{\theta}^{\chi}))^{-\varsigma} \tag{88}$$

where the Lode angle in the generalized stress space $\hat{\theta}^{\chi} = \hat{\theta}^{\chi}(\hat{\boldsymbol{\chi}}) = \frac{1}{3}\arcsin\left[-\frac{3\sqrt{2}}{2}\frac{\hat{J}_3^{\chi}}{(\hat{J}_2^{\chi})^{3/2}}\right]$; $\hat{J}_2^{\chi} = (\chi_q)^2/3 = \hat{\boldsymbol{\chi}}' : \hat{\boldsymbol{\chi}}'/2$; $\hat{\boldsymbol{\chi}}' = \hat{\boldsymbol{\chi}} - \chi_p \mathbf{1}$; $\hat{J}_3^{\chi} = \frac{1}{3}(\hat{\boldsymbol{\chi}}' \cdot \hat{\boldsymbol{\chi}}') : \hat{\boldsymbol{\chi}}'$; while for y^{g^*} we use $M(\boldsymbol{\chi}^*)$ with the necessary changes.

From Eq. (88), it can be seen that the number of parameters increases by two; however, if the parameter ς is taken to be zero, then the Mises failure criterion is invoked again with $\xi = M$ and the number of parameters does not change. If ϕ_0 is taken as the value of the friction angle, determined from the triaxial test in compression, then the Matsuoka–Nakai failure criterion (Matsuoka and Nakai, 1974) can be approximated by substituting $\varsigma = 0.25$, $\xi = \mathrm{Sin}\,\phi_0$, and $\psi = 2\xi(3-\xi^2)/3\sqrt{3}$, where again the number of parameters remains the same, while ϕ_0 replaces M. The transformation between these two parameters may be easily computed from geometrical consideration, and is given by

$$M = \frac{6\,\mathrm{Sin}\,\phi_0}{3 - \mathrm{Sin}\,\phi_0} \tag{89}$$

It is also possible to approximate the well-known Lade criterion (Lade and Duncan, 1975) as well as other criteria, but in the following we adopt the Matsuoka–Nakai criterion.

Since we modified the yield surfaces in (64) and (65), it is important to verify whether the dissipation is still always non-negative. However, according to the convex analysis performed by van Eekelen (1980),

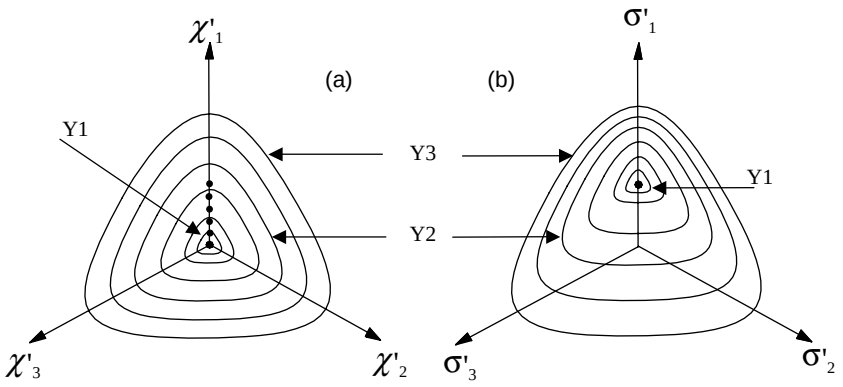

Fig. 4. CHCS field of yield surfaces projection on the octahedral plane.

each of the surfaces in the field is convex in the octahedral plane. Since in the q–p plane the elliptical MCC surfaces are also convex, we conclude that the entire surface shape is convex. Fig. 3(b.2) shows that the generalized yield surfaces always pass through the origin and from Fig. 4(a) we see that they contain the origin in octahedral generalized stress space; hence

$$\boldsymbol{\chi} : \partial y/\partial \boldsymbol{\chi} \geqslant 0 \tag{90}$$

for each surface in the field. Multiplying Eq. (90) by the related non-negative multiplier $\lambda \geqslant 0$, and noting $\dot{\boldsymbol{\alpha}} = \lambda \partial y/\partial \boldsymbol{\chi}$, we observe that $\boldsymbol{\chi} : \dot{\boldsymbol{\alpha}} \geqslant 0$ is always obeyed, which guarantees non-negative dissipation, as in Eq. (6).

The derivatives of the Gibbs potential do not change since only the yield surfaces were modified. The flow rules, though modified, remain associated. The principal shape of the ellipses in Fig. 3 is varied, so that in the three-dimensional view, the entire shape is ellipsoidal with Matsuoka–Nakai cross-sections perpendicular to the hydrostatic axis. For example, the field of cross-sections of the field of yield surfaces is described in Fig. 4 for initial conditions.

8. Parametric study

The CHCS model requires fourteen independent parameters, described below. Though an extensive parametric study is not feasible here due to the lack of space, effects of some of the less conventional parameters on the model behavior in standard triaxial consolidation, swelling and shear conditions are briefly addressed in this section.

8.1. Parameters of the model

Elastic parameters:

$\bar{G}$ the dimensionless shear modulus constant in empirical relation (70)

$\bar{K}$ the dimensionless bulk modulus constant in empirical relation (70); note that the parameter κ^* is not an extra parameter, since it is indirectly defined by $\bar{K}$

n a constant in relation (70)

m a constant in relation (70)

J_0 the inherent elastic coupling modulus constant in (69)

Small-strain parameters:

η_{Y1} the size ratio between Y1 and Y2
x_L the normalized limiting strain at the SSR boundary (Y2)
R_1^K the bulk stiffness reduction within the SSR
R_1^G the shear stiffness reduction within the SSR

Large-strain parameters:

η_{Y2} the size ratio between Y2 and Y3
x_L^G the normalized limiting shear strain between Y2 and Y3
x_L^K the normalized limiting volumetric strain between Y2 and Y3
λ^* inclination of the virgin compression line
ϕ_0 the value of the friction angle determined from the triaxial test in compression

An initial state parameter, p_{y0}, which represents the preconsolidation pressure that defines the initial size of Y3, has to be provided as well.

Provided all the above parameters are defined, the rest of the constants utilized by the proposed model can be easily derived from the corresponding relationships. The model parameters presented herein could all be derived from a single consolidated undrained triaxial compression test instrumented for local deformation measurements. Initially, the soil sample undergoes isotropic compression to point A which lies on the virgin compression line, followed by isotropic swelling to point B (at approximately half the effective pressure, so that $p_B \approx 0.5p_A$). The sample is then left at this stress state for a period of time, sufficient for the field of yield surfaces to center around B according to assumption in Section 6.5. After that, the sample undergoes shearing in undrained triaxial compression until failure is reached.

8.2. Study program

The initial values of the model parameters for the current study are listed in Table 1. Each of these parameters may get a different value in different evaluations; in this case its new value will be specified separately. The limited parametric study presented in this section follows the different loading paths in triaxial test, as described in Fig. 5; this figure also marks the preconsolidation state parameter, p_{y0}, which gets the value of 200 [kPa]; the initial mean effective stress $p'_0 = 100$ [kPa] and the initial shear stress $q_0 = 0$ [kPa].

8.3. Elastic parameters

The parametric study is limited here to the effects of the form of pressure dependency of the elastic shear and moduli in Eq. (70). The values of the parameters m and n are taken equal by setting $m = n = 0, 0.5, 1$; then the corresponding $\bar{G}$ and $\bar{K}$ values are adjusted to always give the same values of $G_0 = 15000$ [kPa] and $K_0 = 45000$ [kPa].

As follows from the compliance matrix in (69), the deviatoric stress–strain curve for loading path IA (Fig. 6(a)) is exactly the same for different sets of parameters. The strain-path, however, is different (Fig.

Table 1
Initial values of the parameters for the study

Parameter	$\bar{G}$	$\bar{K}$	n	m	J_0	η_{Y1}	η_{Y2}
Value	1500	4500	0.5	0.5	0	0	0.5
Parameter	x_L	R_1^G	R_1^K	x_L^G	x_L^K	λ^*	ϕ_0
Value	2.5	0.2	0.2	2.0	4.0	0.1	35°

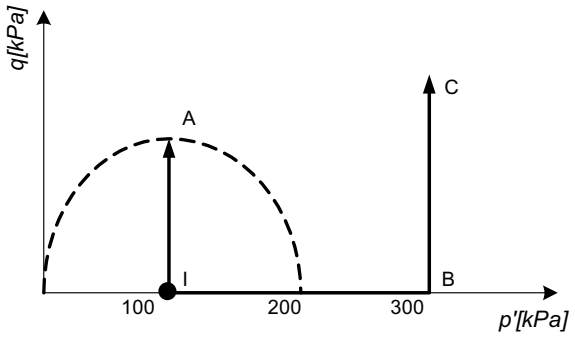

Fig. 5. Test program for the parametric study.

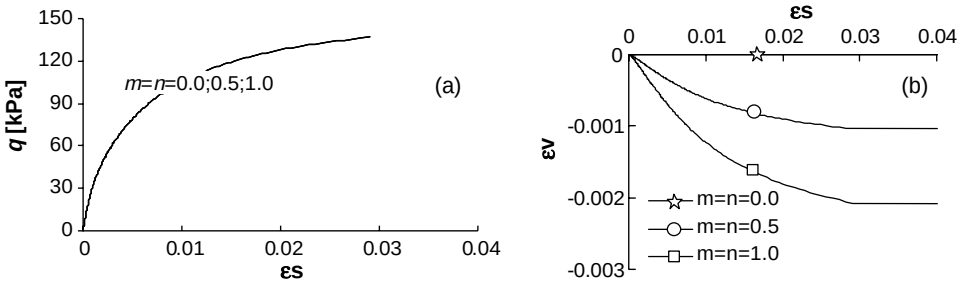

Fig. 6. (a) Deviatoric stress–strain curve and (b) strain-path for drained test IA for different m and n parameters, using the same G_0 and K_0.

6(b)). If $m = n = 0$ than the cross-coupling terms in (69) vanish that is why no volumetric strain is accumulated. When the value of the power dependency is higher, more swelling is experienced. On the other hand, when the same material is subjected to isotropic consolidation (loading path IB), some difference in the stress–strain curves is apparent (Fig. 7), since the bulk stiffness has different pressure dependency. At the end of this consolidation phase both the bulk and shear moduli are not longer equal to their initial values, so that when the material is sheared immediately after the consolidation (loading path BC), the deviatoric stress–strain curves are not identical (Fig. 8). This difference is clearly seen for the small strain secant shear

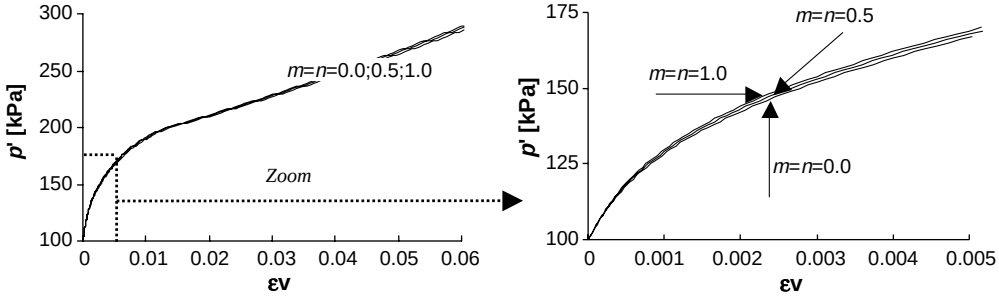

Fig. 7. Volumetric stress–strain curve of isotropic consolidation IB for different m and n parameters, using the same G_0 and K_0.

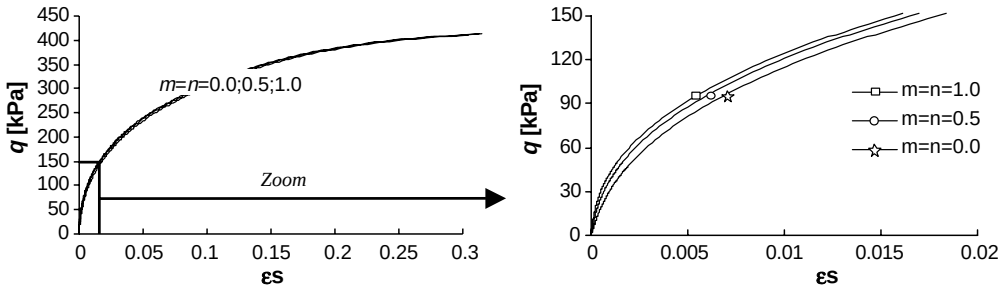

Fig. 8. Deviatoric stress–strain curve for drained test BC for different m and n parameters, using the same G_0 and K_0.

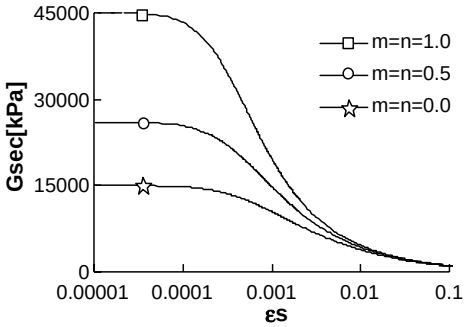

Fig. 9. Degradation of the secant shear modulus for drained test BC for different m and n parameters, using the same G_0 and K_0.

moduli (in triaxial defined by $G_{\text{sec}} = q/3\varepsilon_{\text{s}}$), which then approach the same asymptotic value as the loading progresses towards failure (Fig. 9).

8.4. Small-strain parameters

Next, the effect of the parameter that defines the reduction of stiffness within the small strain region was studied, by making the shear parameter R_1^G vary: $R_1^G = 0.1$, 0.15, 0.2 and 0.25. Fig. 10a and b show how the shear stress–strain curve changes as a result of this variation. It can be seen that this parameter do not alter the strain at the end of the small strain region (Y2) because all the curves meet at this point. However, this parameter affects the strain value at failure since the tangent stiffness at Y2 is different. The strain path variations are shown in Fig. 10c and the secant shear modulus degradation during loading is given in Fig. 10(d). The last figure shows that even while the elastic nucleus is neglected (since $\eta_{\text{Y1}} = 0$), there is some "quasi-elastic" domain which is controlled by the R_1 parameters. This is a known property of the Ramberg–Osgood stress–strain relationship, which is characterized by slow reduction in stiffness and small amount of damping.

Another important parameter is the normalized limiting strain at Y2, x_{L}. Fig. 11 correspond to Fig. 10, though this time—for x_{L}. Fig. 11 highlights how the parameter x_{L} changes the strain within Y2, but unlike R_1 almost does not influence the strain at failure since the tangential stiffness at Y2 is the same. As with the R_1 parameter, x_{L} also controls the size of the "quasi-elastic" domain (Fig. 11(d)). It might be suggested, that a proper choice of the small strain parameters may allow for the Y1 region to be neglected (i.e. $\eta_{\text{Y1}} = 0$), while R_1 and x_{L} will control the "quasi-elastic" domain size.

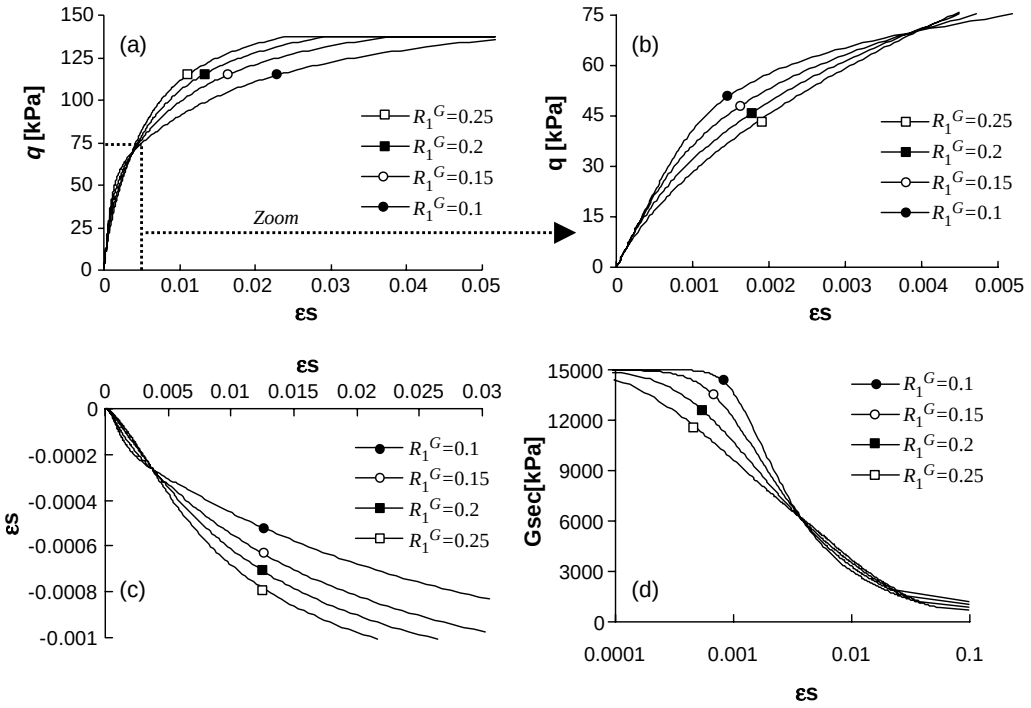

Fig. 10. Study on the R_1^G parameter for drained test IA: (a) stress–strain curve; (b) magnified stress–strain curve; (c) strain path curve and (d) degradation curve of the secant shear modulus.

8.5. Large-strain parameters

Finally, we examine the effects of the normalized limiting strain x_L^G between Y2 and Y3. For brevity, we demonstrate only the variations in shear stress–strain curve for $x_L^G = 2$, 4, 6, 8, and 10. As can be seen in Fig. 12, an increase in this parameter increases the strain to failure.

8.6. Discussion on the choice of parameters

The fourteen independent parameters for the CHCS model were selected to correspond to previous observations and trends in constitutive modeling for clays. The emphasis here is on establishing a conceptual competitive model rather than on suggesting a practical engineering model. In real design and practice, however, the use of such high number of parameters may be unfavorable. It is possible to reduce the number of parameters by assuming some empirical relations based on laboratory tests. Moreover, at this stage, if a smaller number of parameters is desired, then we suggest considering to eliminate the elastic nucleus (i.e. using $\eta_{Y1} = 0$); using the same power dependency $m = n$ for the bulk and shear moduli (thus enforcing a constant Poisson's ratios); their values may also be assumed from the literature.

9. Conclusions

This paper presents a thermodynamically admissible model (CHCS) which is based on a unified hyperplastic formulation. This formulation makes use of the *continuous hyperplastic* component to capture

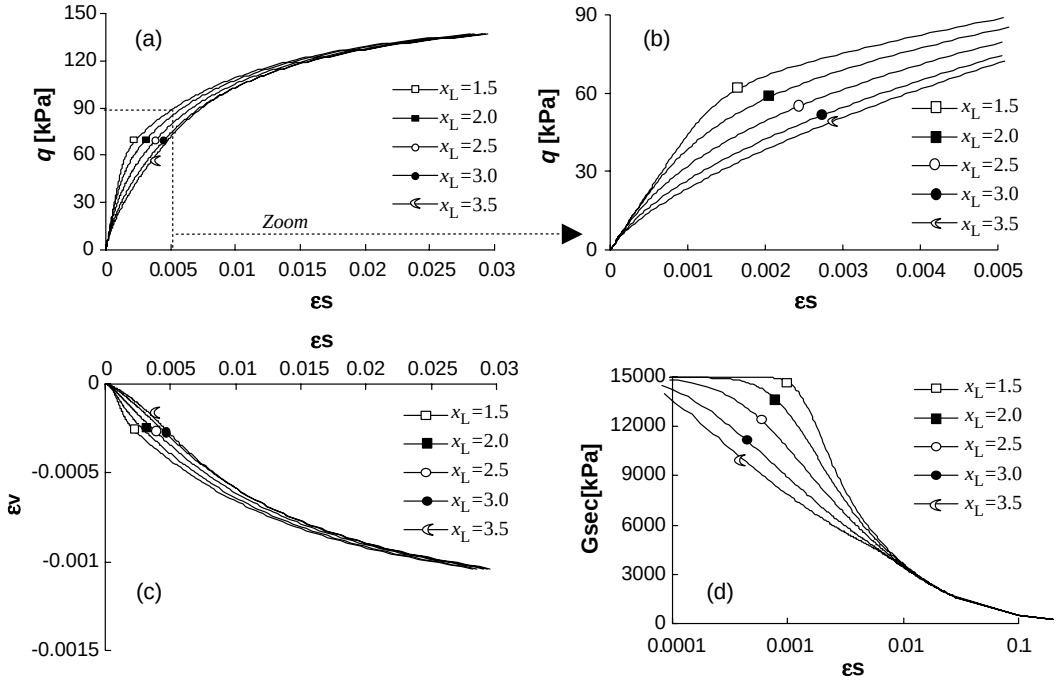

Fig. 11. Study on the x_L parameter for drained test IA: (a) stress–strain curve; (b) magnified stress–strain curve; (c) strain path curve and (d) degradation curve of the secant shear modulus.

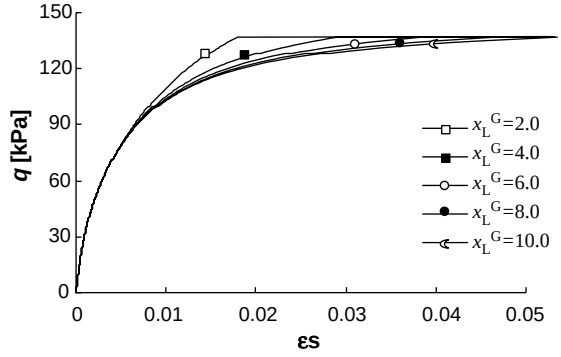

Fig. 12. Deviatoric stress–strain curves for different x_L^G values.

the smooth non-linear kinematic hardening behavior prior to the large scale yielding, while the *hyperplastic* component is used to describe the monotonic isotropic hardening behavior beyond this instantaneous yielding. Although in this work we apply the unified formulation to soils, it could probably find application in modeling of other solid materials, where the abrupt phenomena are combined with general continuous behavior.

The paper also establishes a technique for modeling different kinematic hardening stiffness regions within the above formulation. Using this technique the CHCS model was developed by identifying three kinematic

regions: the hyperelastic region; the small strain region (SSR) where the stiffness reduction is rapid; and the intermediate region. In addition, an isotropic hardening region controls the large scale yielding using a single hyperplastic isotropic-hardening yield surface. The compliance matrix developed by Einav and Puzrin (2003a) governs the hyperelastic region. The stress–strain curve within the SSR is governed by the conventional Ramberg–Osgood function while within the intermediate region it is dominated by a modified hyperbolic function.

The field of yield surfaces is prescribed by the modified Cam Clay elliptical yield surface, with a Matsuoka–Nakai projection on an octahedral plane, which allows us to account for the dependency of yielding on the third stress invariant.

A limited parametric study is presented, with more elaborate evaluation of the model performance against the lab tests and field measurements given in the companion paper.

Acknowledgement

This research was supported by the fund for the Promotion of Research at the Technion.

References

Been, K., Jefferies, M.G., Hachey, J., 1991. The critical state of sands. Geotechnique 41 (3), 365–381.

Borja, R.I., Tamagnini, C., Amorosi, A., 1997. Coupling plasticity and energy-conserving elasticity models for clays. J. Geotech. Geoenviron. Eng. 123 (10), 948–957.

Burland, J.B., 1989. Small is beautiful— the stiffness of soil at small strains. Ninth Laurits Bjerrum Memorial Lecture. Can. Geotech. J. 16 (4), 499–516.

Coleman, B.D., 1964. On thermodynamics of materials with memory. Arch. Rat. Mech. Anal. 17, 1–46.

Coleman, B.D., Gurtin, M.E., 1967. Thermodynamics with Internal state variables. J. Chem. Phys. 47, 597–613.

Collins, I.F., Houlsby, G.T., 1997. Application of thermomechanical principles to the modeling of geomaterials. Proc. R. Soc. London Ser. A 453, 1975–2001.

Einav, I., 2002. Applications of thermodynamical approaches to mechanics of soils. Ph.D. Thesis. Technion, Israel Institute of Technology, Haifa.

Einav, I., Puzrin, A.M., 2003a. Pressure dependent elasticity and energy conservation in elasto-plastic models for soils. ASCEs J. Geotech. Geoenviron. Eng. (accepted).

Einav, I., Puzrin, A.M., 2003b. Continuous hyperplastic critical state (CHCS) model. Evaluation. Géotechnique (accepted).

Einav, I., Puzrin, A.M., Houlsby, G.T., 2003. Numerical studies of hyperplasticity with single, multiple and a continuous field of yield surfaces. Int. J. Numer. Anal. Methods Geomech. (27), 837–858.

Halphen, B., Nguyen Quoc Son, 1975. Sur les matériaux standards généralizés. J. Méc. 14, 39–63.

Hardin, B.O., Drnevich, V.P., 1972. Shear modulus and damping in soils: measurement and parameter effects. ASCE 98 (SM 6), 603–624.

Houlsby, G.T., 1981. A study of plasticity theories and their applicability to soils. Ph.D. Thesis, University of Cambridge.

Houlsby, G.T., Puzrin, A.M., 2000. A thermomechanical framework for constitutive models for rate-independent dissipative materials. Int. J. Plast. 16 (9), 1017–1047.

Jardine, R.J., 1992. Some observation on the kinematic nature of soil stiffness. Soils Found. 32 (2), 111–124.

Jardine, R.J., Potts, D.M., Fourie, A.B., Burland, J.B., 1986. Studies of the influence of nonlinear stress–strain characteristics in soil-structure interaction. Geotechnique 36 (3), 377–396.

Kestin, J., Rice, J.R., 1970. Paradoxes in the application of thermodynamics to strained solids. In: Stuart, E.B., Gal'or, B., Brainard, (Eds.), A Critical Review of Thermodynamics. Mono Book, Baltimore, pp. 275–298.

Kondner, R.L., 1963. Hyperbolic stress–strain response: cohesive soils. ASCE 82 (SM 1), 115–143.

Lade, P.V., Duncan, J.M., 1975. Elasto-plastic stress–strain theory for cohesionless soil with curved yield surfaces. ASCE, GT Div. 101, 1019–1035.

Lubliner, J., 1972. On the thermodynamic foundation of non-linear solid mechanics. Int. J. Non-Linear Mech.

Matsuoka, H., Nakai, T., 1974. Stress-deformation and strength characteristic of soil under three different principal stresses. Proc. JSCE, No. 232, pp. 59–70.

Maugin, G.A., 1992. The Thermomechanics of Plasticity and Fracture. Cambridge University Press.
Puzrin, A.M., Houlsby, G.T., 2001a. A thermomechanical framework for rate-independent dissipative materials with internal functions. Int. J. Plast. 17, 1147–1165.
Puzrin, A.M., Houlsby, G.T., 2001b. Fundamentals of kinematic hardening hyperplasticity. Int. J. Solids Struct. 38, 3771–3794.
Puzrin, A.M., Houlsby, G.T., 2001c. On the non-intersection dilemma in multi-surface plasticity. Geotechnique 51 (4), 369–372.
Ramberg, W., Osgood, W.R., 1943. Description of stress–strain curves by three parameters. Technical Note 902, National Advisory Committee for Aeronautics, Washington, DC.
Smith, P.R., Jardine, R.J., Hight, D.W., 1992. The yielding of Bothkennar clay. Geotechnique 42 (2), 257–274.
Truesdell, C., 1969. Rational Thermodynamics. McGraw-Hill, New York.
Van Eekelen, H.A.M., 1980. Isotropic yield surfaces in three dimensions for use in soil mechanics. Int. J. Num. Anal. Meth. Geomech. (4), 89–101.
Ziegler, H., 1977. An Introduction to Thermomechanics. North Holland, Amsterdam (2nd edition, 1983).